MODELING THE SOLVENT EFFECT IN FREE RADICAL POLYMERIZATION AND DEAMIDATION OF PEPTIDES

by

Berna Doğan

B.S., Chemistry, Boğaziçi University, 2011

Submitted to the Institute for Graduate Studies in
Science and Engineering in partial fulfillment of
the requirements for the degree of
Master of Science

Graduate Program in Chemistry

Boğaziçi University

2012

To my family…

ACKNOWLEDGEMENTS

I would like to express my sincere gratitude to my thesis advisor Prof. Viktorya Aviyente for her endless support and patience throughout my studies. I would like to thank her for everything that I learned from her. It is always a great pleasure for me to be her student.

I wish to thank to the members of my committee: Assoc. Pror. Amitav Sanyal and Assoc. Prof. Nurcan Tüzün for giving their valuable time and advices.

I would like to thank to all the members of computational chemistry family, especially to İlke Uğur, Tuğba Furuncuoğlu-Özaltın and İsa Değirmenci for introducing me to computational chemistry. In addition, I would like to specifically thank Aslı Yıldırım, Özlem Karahan, Hasan İnce, Gülşah Çifci, Burcu Dedeoğlu and Sesil Agopcan for their friendship and support. I am also grateful to Hülya Metiner for her invaluable helps.

I gratefully acknowledge Prof. Michel Waroquier, Prof. Dr. ir. Veronique Van Speybroeck and Dr. Saron Catak for their advices, comments, scientific guidance during my stay in Ghent, Belgium.

I also want to thank my dear friends; Merve Coşar, Esra Cabalar, Havva İlbey, Işıl Kaya and Funda Ekşi for their sincere friendship and support, glad to have all of them in my life.

My greatest thanks and love of course go to my family; my mother Birsel, my father Ahmet and my sisters Ebru and Beyzanur for their continuous, sincere and genuine support and love throughout my life.

ABSTRACT

MODELING THE SOLVENT EFFECT IN FREE RADICAL POLYMERIZATION AND DEAMIDATION OF PEPTIDES

In the first part of this study, the kinetics free radical polymerization of ethyl methacrylate (EMA) and ethyl α-hydroxy methacrylate (EHMA) in solution is investigated; in the second part the deamidation in three different dipeptides is modeled in solution by using Density Functional Theory (DFT).

In the first part of this study, the propagation kinetics of EMA and EHMA has been subjected to a computational study in order to understand their free radical polymerization (FRP) behavior in bulk and in solution. Methacylates are among the most commonly used monomers in FRP and can be used as dental materials, biomaterials, adhesives, optical adhesives, coatings, fiber-optic coatings and in many other areas. The hydroxy-functional methacrylate monomers have drawn attention due to their hydrophilicity, crosslinking sites and functionality for subsequent reactions. The correlation between the calculated propagation rate constants and the experimental results has been reproduced with the MPWB1K/6-311+G(3df,2p) methodology.

In the second part of this study, the deamidation reaction mechanism in peptides is investigated. Out of the twenty naturally occurring amino acid residues, two of them, namely Asparagine (Asn) and Glutamine (Gln) are known to be unstable under physiological solvent conditions. The amide group from the backbone of the amino acid residue of Asn and Gln cleaves to form Aspartly (Asp) and Glutamyl (Glu) residues. Peptides and proteins that contain Asn and/or Gln with different primary sequence are known to have very different half-life times for deamidation. Therefore, the effect of the primary sequence on deamidation is studied by choosing three different peptides as models.

ÖZET

SERBEST RADİKAL POLİMERİZASYONU VE PEPTİTLERİN DEAMİDASYONUNUN MODELLENMESİ

Bu çalışmanın ilk kısmında, etil metakrilat (EMA) ve etil α-hidroksil metakrilatın (EHMA), çözücü içindeki serbest radikal polimerizasyonları; ikinci kısımda ise üç farklı dipeptitin çözücü içindeki deamidasyonları Yoğunluk Fonksiyonları Teorisi (DFT) ile incelenmiştir.

Bu çalışmanın birinci kısımda, EMA ve EHMA monomerlerinin yoğun ortamda ve çözücü içindeki serbest radikal polimerleşmesi davranışını anlamak için yayılma kinetikleri modellendi. Metakrilatlar serbest radikal polimerleşmesinde genel olarak kullanılan monomerler arasındadır ve diş malzemesi, bio malzeme, yapıştırıcı, optik yapıştırıcı, astar, optik-lif astar ve birçok başka özeliklerde kullanılabilirler. Hidroksil fonksiyonelli metakrilatlar ise hidrofilik olmaları, çapraz bağlanma yapabilmeleri ve daha sonraki tepkimeler için fonksiyonel olarak kullanılabilmeleri sebebiyle ilgi çekiyorlar. Monomerlerin hesaplanan yayılma hız sabitleri ve deneysel hız sabitleri arasındaki eğilim, en uyumlu olarak MPWB1K/6-311+(3df,2p) yöntemiyle bulunmuştur.

Bu çalışmanın ikinci kısımda, peptitlerdeki deamidasyon tepkimeleri incelendi. Doğada bulunan yirmi tane amino asit arasında iki tanesi, asparajin (Asn) ve glutaminin (Gln) fizyolojik ortamda istikrarlı olmadıkları bilinmektedir. Amino asit kalıntısının arka omurgasındaki amid grubu kırılak aspartik asit (Asp) ve glutamik asit (Glu) oluşturur. Asn ve/veya Gln içeren peptit ve proteinlerin de farklı birincil yapıları var ise, deamidasyon yarılanma zamanlarının da çok farklı olduğu bulunmuştur. Bu sebeple, bu çalışmanın ikinci kısmında farklı üç peptit model olarak seçilerek birincil yapının deamidasyon üzerindeki etkisi çalışılmıştır.

TABLE OF CONTENTS

LIST OF FIGURES

LIST OF TABLES

LIST OF SYMBOLS/ABBREVIATIONS

$\Delta G^{\ddagger}$	Gibbs free energy of activation
B3LYP	Becke-3-parameter Lee-Yang-Parr functional
BMK	Becke-Martin for kinetics
DFT	Density functional theory
GGA	Generalized gradient approximation
HF-DF	Hartree-Fock-density functional
IEF-PCM	Integral equation formalism model polarizaed continuum model
M06-2X	Minnesota 2006 hybrid with doubled portion of HF exchange
MPW1K	Modified Perdew-Wang 1 Parameter Method for Kinetics
UFF	Universal Force Field
k_i	Rate constant for initiation
k_p	Rate constant for propagation
k_t	Rate constant for termination
k_{tr}	Rate constant for chain transfer

1. INTRODUCTION

1.1. Free Radical Polymerization

Free radical polymerization (FRP) is one of the most widely used reactions, since it enables the synthesis of high molecular weight polymers from a variety of monomers [1, 2]. Due to its wide applicability, understanding the mechanism of FRP has become a common goal for both experimentalists and theoreticians [3].

The polymerization of unsaturated, mostly double bonded monomer unit is a chain reaction in FRP. These chain reactions can be basically categorized into three different types of reactions involving radicals:

i. Initiation
ii. Propagation
iii. Termination

Free radicals may be produced when a labile organic compound (initiator), I_2, is decomposed by light or particulate radiation to produce radicals, R:

$$I_2 \xrightarrow{k_d} 2R\bullet \tag{1.1}$$

where k_d is the dissociation rate constant of the initiator [4]. In the second part of the initiation, the radical formed from the initiator attacks to the monomer in the media:

$$R_1\bullet + M \xrightarrow{k_i} M_1\bullet \tag{1.2}$$

where k_i is the initiation step rate constant and M represent monomer and M_1 is an initiator species. The kinetics of the initiation step is of uttermost important in both theoretical and commercial applications since it is the first step for FRP [4].

After the formation of initiators, FRP proceeds by the formation of macroradicals: the propagation step. In this step initiating species, M_1 attacks to other monomers and are added to them, forming a chain. The growth of this chain by the successive additions may continue up to hundreds or thousands of monomer units forming "polymers". Below is the schematic representation for propagation step:

$$M_n\bullet + M \xrightarrow{k_p} M_{n+1}\bullet \tag{1.3}$$

here k_p represent the propagation rate constant and since 1990 there has been special interest for accurate determination of this constant. The propagation takes very rapidly and rate constant is known to be affected by polarity, resonance, medium and steric factors [5].

The last step of FRP is termination which is the most complex reaction in the polymerization process since termination rate constant, k_t, is influenced by a multitude of different factors [5]. The propagation may end up by two different modes of terminations: (1) direct coupling/combination of two free radicals, macroradicals via a bimolecular reaction that result in a saturated dead polymer chain (shown below in 1.4).

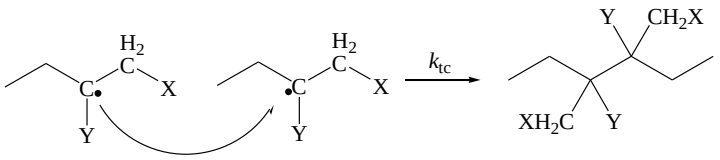

(1.4)

and (2) the so called disproportionation in which a hydrogen that is beta to a radical center is transferred to another radical center. This time one saturated and one unsaturated dead polymer chains are obtained (shown below in 1.5).

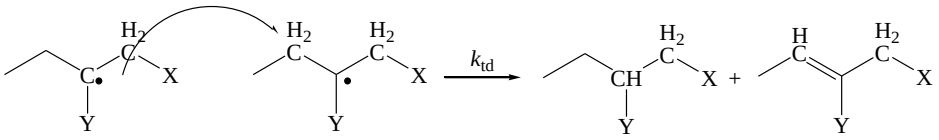

(1.5)

where k_{tc} is the rate constant for termination by combination and k_{td} by disproportionation. X and Y are the pendant groups of the monomer used. These two reactions can be depicted by

$$M_n\bullet + M_m\bullet \xrightarrow{k_{tc}} M_{n+m} \tag{1.6}$$

$$M_n\bullet + M_m\bullet \xrightarrow{k_{td}} M_n + M_m \tag{1.7}$$

where the termination rate constant is expressed by the sum of rate constants of the two reactions as

$$k_t = k_{tc} + k_{td} \tag{1.8}$$

Among these steps, the propagation step is particularly important since other rate coefficients can be obtained coupled to k_p like the chain transfer constant, C_T and/or the termination rate constant k_t [6]. Additionally, knowing the k_p, one can control the propagation step and the degree of monomer conversion. Experimentally, it became possible to measure k_p after the pioneering work of Olaj and Schnöll-Bitai [7, 8] on pulsed laser initiated polymerization (PLP) and subsequent analysis of the polymer by size exclusion chromatography (SEC). The so-called PLP-SEC technique emerged as the most powerful technique to derive individual propagation rate coefficients independently of the other coefficients and it is also possible to measure k_p in solvent. Consequently, it is important to understand what affect the k_p both in bulk and solvents to control FRP.

1.2. Deamidation in Peptides and Proteins

The two of the natural occurring amino acids, Asparagine (Asn) and Glutamine (Gln) are known to be unstable under physiological solvent conditions [9]. The side chain amide group of the amino acid residue of Asn and Gln cleaves to form Aspartly (Asp) and

Glutamyl (Glu) residues. Asn and Gln were shown to be normal constituents of proteins and were first studied with respect to deamidation [10-12].

The deamidation of peptides and proteins, due to the Asn and/or Gln residues is known to cause degradation and produce protein defects [9]. This can be problematic during the storage, transformation and purification of proteins and peptides. However more importantly, deamidation reactions have also been observed in *vivo* as a post-translation modification which makes the study of deamidation reactions of Gln and Asn important.

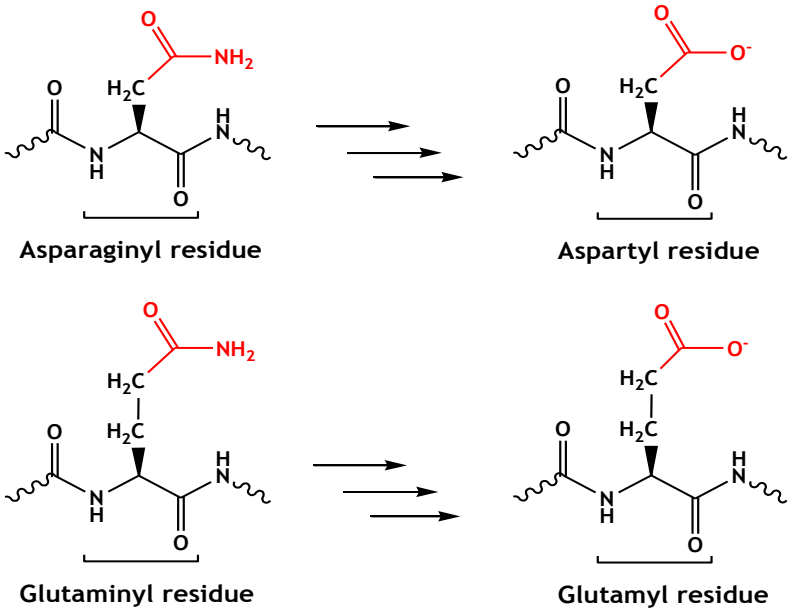

Figure 1.1. Deamidation of asparaginyl and glutaminyl residues.

Nonenzymatic deamidation of Asn or Gln residues in *vivo* or in *vitro* under physiological solvent conditions has been reported for more than 200 types of naturally occurring peptides and proteins [9, 13]. Most of these molecules deamidate primarily at Asn residues, including those of special current interest such as ribonuclease and phenylalanine hydroxylase [14]. It is known that deamidation rates of Glu are much slower compared to Asn residue and therefore, nonenzymatic deamidation of Gln has been observed primarily in very long-lived proteins such as the crystallines of the eye lens [14].

It has been hypothesized by Robinson *et al*. that deamidation of Asn and Gln residues serves as general timer for the regulation of biological processes [15]. They have determined the deamidation rates of peptides and proteins and these rates demonstrate that

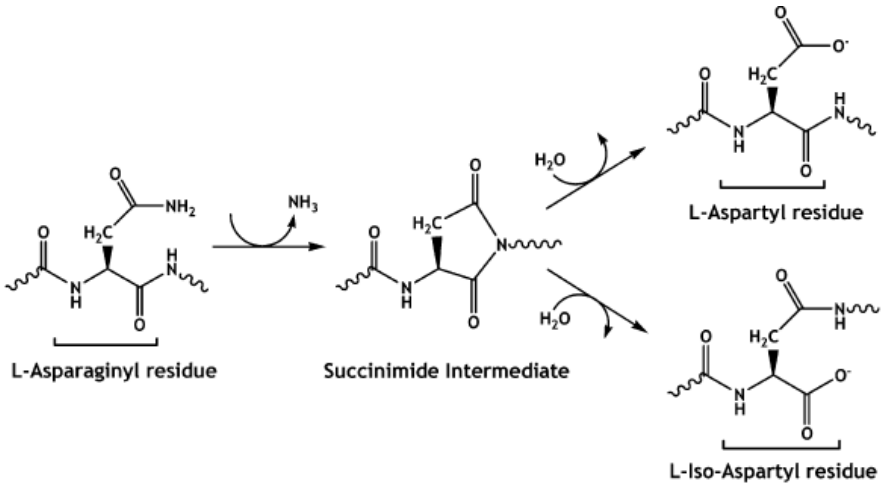

Figure 1.2. Deamidation through succinimide intermediate.

deamidation provides molecular clocks that are suitable for the regulation of aging, development, and other biochemical processes. Increased amounts of deamidated proteins have been found in some aged and diseased tissues, such as human eye lens cataracts [16] and Alzheimer's plaques [17].

Deamidation of Asn in peptides and proteins is moderately well understood. At physiological pHs, this reaction apparently proceeds primarily through formation of a five member cyclic imide intermediate (Figure 1.2). At acidic pH or at neutral to basic pH in those instances when imide formation is structurally prevented, Asn deamidation apparently proceeds primarily through general acid and general base catalyzed hydrolysis [14]. Also it is known that, at acidic pH the cyclization step is rate determining, whereas, the removal of the leaving group by apparent general-base catalysis is the rate-determining step at neutral and basic pH.

Deamidation rates in peptides and proteins are known to be influenced by primary structure, i.e. the peptide sequence near the Asn residue [14]. Robinson *et al*. claimed by their methods that the deamidation rate of peptides and proteins depends 60% on primary

structure and 40% on three-dimensional structure. In addition to that finding, it has also been shown that protein deamidation rates are about the same as pentapeptide models for amides in unhindered regions of the protein [18]. By using pentapeptides as their model structures of proteins, Robinson *et al*. showed that sequence of the peptide affects the deamidation half-life times of the peptide, the range changes from less than a day to more than a century depending on the sequence [19]. Consequently, it is desirable to understand the reason of this sequence effect.

2. FREE RADICAL POLYMERIZATION OF ETHYL METHACRYLATE AND ETHYL α-HYDROXY METHACRYLATE: A COMPUTATIONAL APPROACH TO THE PROPAGATION KINETICS

2.1. Introduction

Acrylates and methacrylates are among the most commonly used monomers in FRP. They can be used as dental materials, biomaterials, adhesives, optical adhesives, coatings, fiber-optic coatings, aspherical lenses for CD applications, contact lenses and photolithography [20-22]. Recently, hydroxy-functional acrylic and methacrylate monomers have been studied both experimentally and theoretically [23-33] due to their hydrophilicity, crosslinking sites and functionality for subsequent reactions.

It is known that ester derivatives of α-hydroxymethacrylates –RHMA's– show fast photopolymerization rates both on their own and in the presence of acrylate or methacrylate crosslinkers [34]. The ester group's effect on the free radical polymerization of α-hydroxymethacrylates has been theoretically investigated [29] and the polymerization rate was shown to be correlated to the steric hindrance caused by the alkyl substituents. More specifically, the bulky alkyl group in *t*-butyl α-hydroxymethacrylates (TBHMA) was suggested to inhibit propagation when compared to the smaller alkyl groups in ethyl α-hydroxymethacrylates (EHMA) and methyl α-hydroxymethacrylates (MHMA) and the trend in k_p's for α-hydroxymethacrylates was calculated as: k_p(MHMA) > k_p(EHMA) > k_p(TBHMA) [27]. Furthermore, in the case of MHMA, a rate enhancing effect of the intermolecular hydrogen-bonding between propagating radicals was reported [29].

In recent years, there is an increased interest in the development of bioactive polymeric dental composites and related materials that have the potential for mineralized tissue regeneration and preservation. Ethyl α-hydroxy methacrylate (EHMA) is known to have acceptable ion releasing properties and is considered a suitable substitute for 2-

hydroxy methacrylate (HEMA), a structural isomer of EHMA, in dental and possibly biomedical applications due to its smaller water affinity [35]. Random copolymerization of EHMA with styrene and methacrylate yields polymers that have potential applications as biomaterials [36]. Furthermore, EHMA can be utilized in catalytic chain transfer polymerization –an effective technique to control the molecular weight in FRP [37].

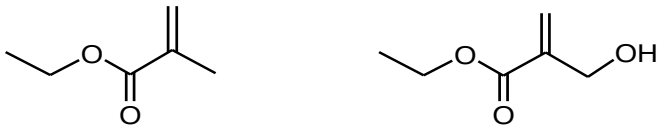

EMA EHMA

Figure 2.1. Structures of ethyl methacrylate (EMA) and ethyl α-hydroxymethacrylate (EHMA).

Due to the potential bio-applicability, the polymerization behavior of EHMA has been subject to several experimental studies. Davis *et al.* have used Pulsed Laser Polymerization (PLP) technique to measure the propagation rate constant (k_p) of EHMA in different solvents; however, due to chain transfer, k_p of EHMA in bulk was not successfully measured [31]. However, the variation of k_p in different solvents was found to be substantially larger than that previously observed for any other acrylic or styrenic monomer. On the other hand, the polymerization behavior of ethyl methacrylate (EMA) –a monomer extensively used in the contact lens industry due to its ease of polymerization with radical initiators [38] – was successfully studied by Zammit *et al.* by PLP in bulk [33]. The comparison of propagation rate constants of the two polymers shows that EHMA k_p values are 12-40% times higher than those for EMA [31, 33]. Higher k_p values for EHMA are actually surprising, since the hydroxymethyl group is bulkier than the methyl group; it is suggested that this is caused by the hydroxyl group's electronic influence on the radical center and/or on the EHMA monomer reactivity. Similarly, Ueda *et al.* [32] have reported that introducing heteroatoms into the methyl group increases the reactivity of these monomers due to inductive effects. Nevertheless, the effect of hydrogen bonding on polymerization kinetics should also be taken into consideration, since EHMA is prone to intermolecular hydrogen-bonding through its hydroxyl group (Figure 2.1). Many experimental studies report that monomers with hydrogen bonding capability have higher

polymerization rates compared to their non-hydrogen bonding analogues [39-42]. In fact Hoyle *et al.* [41] have shown by FTIR that hydrogen bonds are present during hydroxyalkyl acrylate polymerization and the rate is directly related with hydrogen-bond formation. This increase in polymerization rate is attributed to both the increase in propagation rate and the decrease in termination rate.

Recently, the effect of solvent on the free radical polymerization kinetics, conversion and regularity has been studied [6, 25, 26, 43-45]. Beuermann *et al.*, particularly emphasized the influence of organic solvents on the propagation rates of monomers with hydroxy functionality [6]. It was concluded that in the case of non-hydrogen bonding solvents –solvents that cannot form hydrogen bonds with the monomer or the macromolecular species– the relative size of the solvent as compared to the monomer governs whether k_p will be higher or lower than its value in bulk. It is shown that effect of solvent (ones that are not able to form hydrogen bonds) is higher when the sizes of monomer and solvent are far different than each other; and the effect is lower almost nonexistent if the sizes of monomer and solvent are close to each other. For hydrogen-bonding solvents, which can form hydrogen bonds with the monomer or the propagating radical, the effect of H-bonding on reactivity should be explicitly considered.

Davis *et al.* [31] have monitored the free radical polymerization kinetics of EHMA in three different solvents, namely, toluene, tetrahydrofuran (THF) and ethanol. It was found that in the case of ethanol and THF (polar solvents with hydrogen-bonding capacity), k_p decreases upon increased solvent ratios, whereas an increase in k_p is observed when the amount of toluene (non-hydrogen bonding hydrophobic solvent) was increased (Table 2.1). These findings have been attributed to special interactions between the solvent and the propagating species in the case of ethanol and THF.

Herein, the propagation reaction of EMA and EHMA is subject to a computational study in order to understand their polymerization behavior and the effect of the α-hydroxy functionality. Moreover, hydrogen-bonding modes of EHMA –intramolecular and intermolecular– and their effect on the propagation kinetics will be thoroughly investigated both in bulk and in solution. For this purpose, a hydrogen-bonding solvent, ethanol and a

hydrophobic solvent, toluene, have been chosen and results are rationalized based on the experimental data of Davis *et al*. [31].

Table 2.1. Kinetic parameters for EMA [33] and EHMA [31] obtained from experiment. Activation energies (E_a), pre-exponential constants (A) obtained in the temperature range 283-313K; propagation rate constants (k_p) at 303K for EHMA and at 301K for EMA.

Monomer	Monomer /Solvent (w/w)	E_a (kcal mol^{-1})	A (10^6 L mol^{-1}s^{-1})	k_p (L mol^{-1}s^{-1})	Relative k_p
EHMA	Toluene 3:1	3.85	0.84	1331	1.52
	Toluene 1:1	4.80	4.50	1496	1.71
	Toluene 1:3	4.73	5.47	2098	2.40
	Ethanol 3:1	3.49	0.34	1047	1.20
	Ethanol 1:1	4.95	3.64	950	1.09
	Ethanol 1:3	4.95	3.27	875	**1.00**
EMA	Bulk	5.71	4.45	307	0.35

2.2. Computational Detail

Density Functional Theory (DFT) [46] with the Gaussian 03 [47] program package is used for gas phase calculations. For calculations in solution, the Gaussian 09 [48] program package is used, since it provides significantly enhanced solvation features. Geometry optimizations are carried out with B3LYP/6-31+G(d) [49, 50] for all monomers, radicals and transition states. Harmonic vibrational frequencies were computed at the same level of theory and used to provide thermal corrections to the Gibbs free energies, and to confirm the nature of the stationary points. DFT functionals BMK [51] and MPW1K [52] have been employed for energy refinement. BMK (Becke-Martin for kinetics), a hybrid meta-GGA model, is considered to be a reliable general-purpose functional whose capabilities have

been expanded to cover transition states [51]. MPW1K, also a hybrid Hartree-Fock-density functional (HF-DF), reduces the mean unsigned error in reaction barrier heights by a factor of 2.40 and predicts barrier heights more accurately than other widely used methods [52].

The conventional transition state theory (TST) [53-56] is used to calculate the rate constant for the bimolecular reaction as follow:

$$k_2 = \kappa \frac{kT}{h} \frac{RT}{p^\theta} e^{-\Delta G^\ddagger / RT}$$

In this equation k represents Boltzmann's constant, T is the temperature, h is Planck's constant, $\Delta G^\ddagger$ represents the Gibbs free energy difference between the activated complex and the reactants, R is the universal gas constant, κ is the transmission coefficient which is assumed to be about 1 and p^θ is the standard pressure 10^5 Pa (1 bar).

The reaction kinetics of EMA and EHMA are compared initially in the gas phase and then by using a dielectric continuum model, namely, the integral equation formalism model (IEF-PCM) [57-59] with UFF radii. In continuum solvation models, the solvent is represented as a polarizable medium characterized by its static dielectric constant ε and the solute is embedded in a cavity surrounded by this dielectric medium [60]. For calculations in bulk, the dielectric constant of EMA has been replaced by the one of methyl methacrylate (MMA) (ε=3.00) based on the lack of information on the former and the similarity of EMA to MMA. Due to the lack of experimental information the dielectric constant of EHMA has been taken as 7.80, which is the dielectric constant of methyl α-hydroxy methacrylate (MHMA). The effect of the solvent on the free radical polymerization kinetics of EHMA was calculated by employing both an implicit (toluene and ethanol) and a mixed implicit/explicit [61, 62] solvation model (for ethanol only). Implicit models which include additional terms for the nonelectrostatic contributions of the solvent, such as dispersion, repulsion, and cavitation, are generally thought to be reliable only when explicit solute - solvent interactions (e.g., hydrogen bonds) are not present. Since EHMA, is capable of hydrogen bonding with ethanol, the solvent effect with ethanol has been considered explicitly. On the other hand, the effect of non-hydrogen bonding

solvents like toluene has been taken into account with continuum solvation models due to the lack of explicit interactions between the solute and the solvent.

Corrections for basis set superposition errors (BSSE), [63] were calculated at each level of theory. Gibbs free energies of activation are calculated as the sum of the electronic energy, the thermal corrections to Gibbs free energy and the BSSE correction. In solution, the free energy of activation is calculated as the sum of electronic energies in solution, thermal correction to Gibbs free energy from gas phase, BSSE correction from gas phase and also a correction term, *RT* ln (24.46), to take into account the conversion from 1 mol L^{-1} (gas) to 1 mol L^{-1} (solution) [64]. Energies reported are in kcal mol^{-1}, propagation rate constants (k_p) are in L $mol^{-1}s^{-1}$. All calculations were done at 303 K.

Rotational potential energy scans around the forming bond are performed in order to locate the energetically most stable transition states [65]. The weighted average of the Gibbs free energies of activation, $< \Delta G^{\ddagger} >$, were calculated by taking into account the Boltzmann distribution (shown below) of each state (each transition state) for EHMA and EMA both in gas phase and in solution.

$$< \Delta G^{\ddagger} > = \sum_{i=1}^{n} \Delta G_i^{\ddagger} \left(\frac{N_i}{N_T}\right)$$

Where $\frac{N_i}{N_T} = \frac{e^{-\Delta(\Delta G_i^{\ddagger})/RT}}{\sum_{i=1}^{n} e^{-\Delta(\Delta G_i^{\ddagger})/RT}}$ and $\Delta G_i^{\ddagger}$ is the Gibbs free energy of activation of the i^{th} state and $\Delta(\Delta G_i^{\ddagger})$ is the difference between the Gibbs free energy of activation of the i^{th} state and the most populated (most stable) state.

2.3. Results and Discussion

Both syndiotactic and isotactic dimeric chains were used to study the propagation step in the FRP of EMA and EHMA. Ethanol and toluene were used as solvents in modeling the polymerization of EHMA.

2.3.1. Propagation of EMA

Based on a conformational analysis carried out for EMA (Figure 2.2), the *trans* monomer and the *syn* radical of EMA are found to be slightly more stable than their counterparts. The *trans* conformer of methyl methacrylate, MMA, is shown to be more favorable due to long range interactions between the methyl group and the carbonyl group of the monomer [28]. Similarly, in EMA four H atoms interact with the carbonyl oxygen in the *trans* conformer, however, only three such interactions are present in the *cis* conformer, so the *trans* conformer is slightly more stabilized. In the EMA radical, EMA-R, the difference between relative energies is even smaller. Since the stabilizing interactions of the carbonyl oxygen atom are almost identical, there is only a weak interaction between the oxygen atom and the ethyl H-atom in the *syn* conformer, which is absent in the *anti* conformer, this makes the *syn* conformer slightly more stable (Figure 2.2).

The radical's direction of attack is of utmost importance because it determines the tacticity of the polymer chain: isotactic, syndiotactic or atactic. In Figure 2.3, the *syn* radical's four different attack modes to the s-*cis* and the s-*trans* monomers are shown; with the inclusion of the *anti* radical, eight different attack conformations have been located for EMA (Table 2.2, Figure 2.4).

Transition state structures are shown in Figure 2.2 along with relative Gibbs free energies. The critical distances in all transition structures are similar. TS-EMA-1, TS-EMA-2, TS-EMA-5 and TS-EMA-6 are stabilized by interactions between the carbonyl oxygen and alkyl group hydrogens. These structures are slightly more stable than the ones which do not have the latter stabilizing interactions. Since the same monomer and radical (EMA-anti and EMA-R-syn) are used in all calculations, the activation energies in Table 2.2 depict the relative stabilities of the transition structures, which are very close in energy to each other. The average $\Delta G^{\ddagger}$ is calculated by using the Boltzmann weighted average formula; both functionals yield similar results. In addition, experimental evidence suggests that in EMA polymerization stereoregularity is syndiotactic [66].

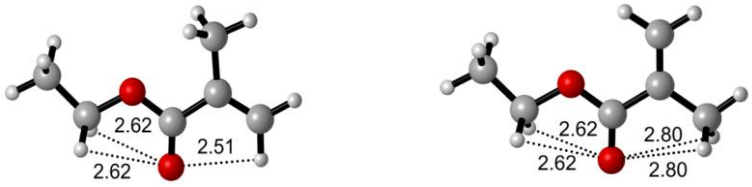

Monomers	EMA-s-*cis*	EMA-s-*trans*
	0.41 (0.35)	0.00 (0.00)*

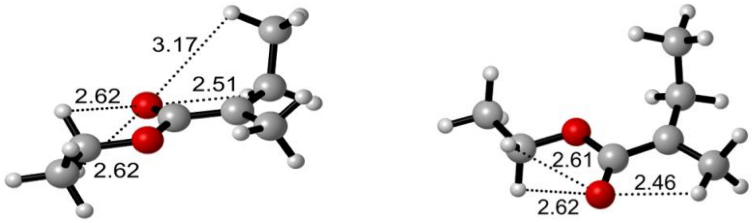

Radicals	EMA-R-*syn*	EMA-R-*anti*
	0.00 (0.00)**	0.14 (0.10)

Figure 2.2. Structures and relative Gibbs free energies of the EMA monomer and radical, EMA-R. IEF-PCM (ε=3.00 for EMA bulk) calculations in parenthesis. MPW1K/6-311+G(3df,2p)//B3LYP/6-31+G(d)). *(HF+ZPG) = -384.997385 kcal mol^{-1} in gas, -385.000753 kcal mol^{-1} in bulk, ** (HF+ZPG) = -424.868016 kcal mol^{-1} in gas, -424.871471 kcal mol^{-1} in bulk.

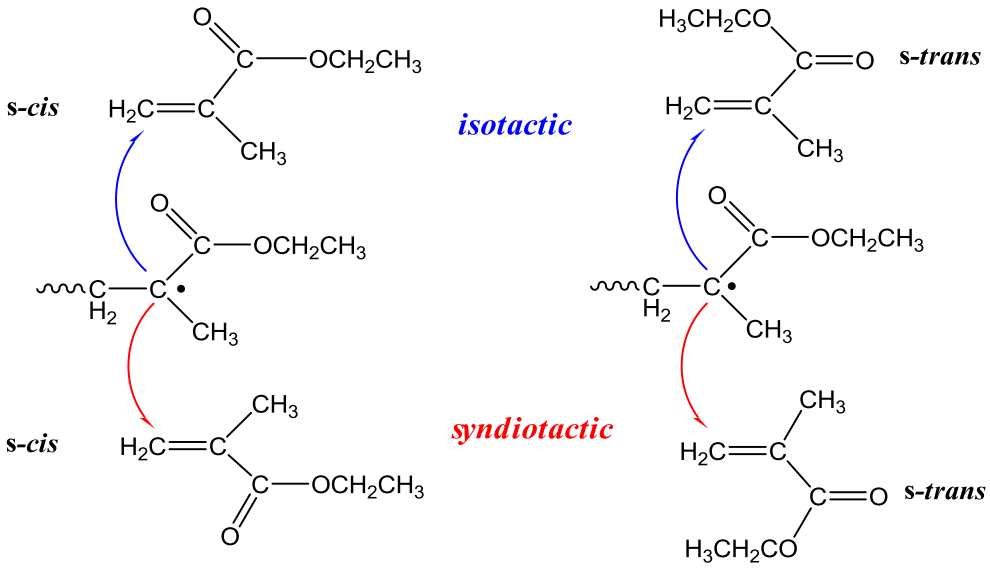

Figure 2.3. *Syn*-radical addition to s-*cis* and s-*trans* EMA.

Table 2.2. Gibbs free energies of activation (kcal mol^{-1}) of EMA at 303K.[a,b]

				$\Delta G^{\ddagger}$	
	Tacticity	Monomer	Radical	BMK[c]	MPW1K[d]
TS-EMA-1	syndiotactic	*cis*	*anti*	21.14 (19.85)	21.59 (20.30)
TS-EMA-2	syndiotactic	*cis*	*syn*	20.89 (19.74)	21.78 (20.63)
TS-EMA-3	syndiotactic	*trans*	*anti*	21.90 (20.34)	22.32 (20.76)
TS-EMA-4	syndiotactic	*trans*	*syn*	21.89 (20.40)	22.10 (20.61)
Weighted Average	syndiotactic			21.15 (19.95)	21.80 (20.53)
TS-EMA-5	isotactic	*cis*	*anti*	20.98 (19.77)	21.81 (20.60)
TS-EMA-6	isotactic	*cis*	*syn*	21.09 (19.86)	21.55 (20.33)
TS-EMA-7	isotactic	*trans*	*anti*	21.87 (20.32)	22.24 (20.69)
TS-EMA-8	isotactic	*trans*	*syn*	21.54 (20.07)	22.03 (20.56)
Weighted Average	isotactic			21.19 (19.94)	21.79 (20.52)
Weighted Average	Overall			21.17 (19.94)	21.80 (20.52)

[a]BSSE corrections included. [b]IEF-PCM (ε=3.00 for bulk EMA) calculations in parenthesis. [c]BMK/6-311+G(3df,2p)//B3LYP/6-31+G(d). [d]MPW1K/6-311+G(3df,2p)//B3LYP/6-31+G(d).

Syndiotactic	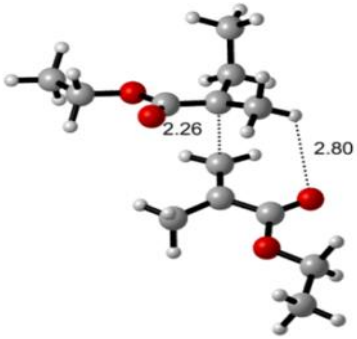	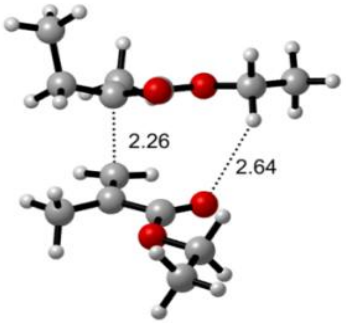	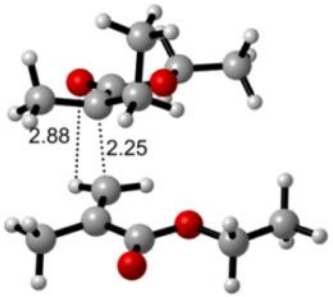	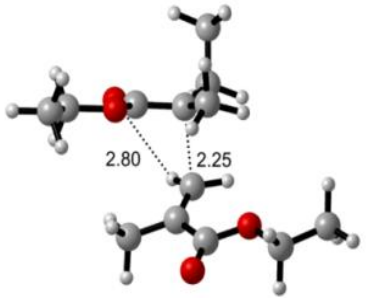
	TS-EMA-1	TS-EMA-2	TS-EMA-3	TS-EMA-4
	0.03 (-0.03)	0.22 (0.29)	0.77 (0.43)	0.54 (0.28)
Isotactic	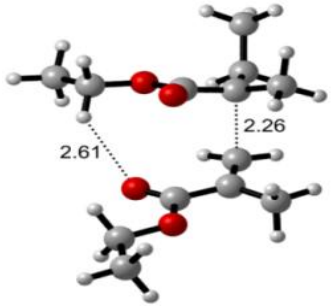	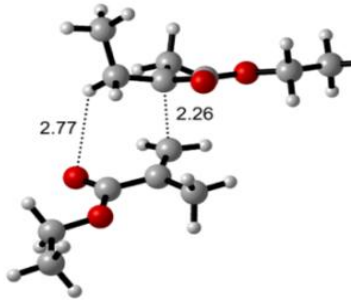	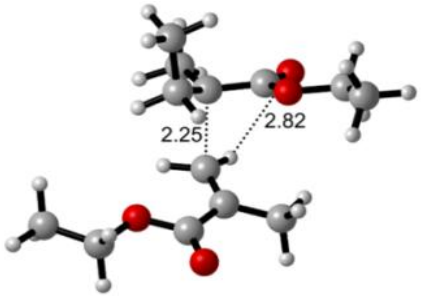	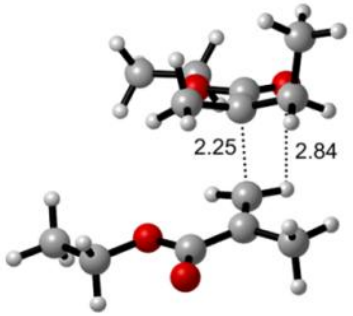
	TS-EMA-5	TS-EMA-6	TS-EMA-7	TS-EMA-8
	0.26 (0.26)	0.00 (0.00)*	0.68 (0.36)	0.48 (0.22)

Figure 2.4. Structures and relative Gibbs free energies (BSSE corrections included) of the transition states of EMA.

IEF-PCM (ε=3.00 for bulk EMA) calculations in parenthesis. MPW1K/6-311+G(3df,2p)//B3LYP/6-31+G(d). * (HF+ZPG) is -809.831054 kcal mol^{-1} in gas, -809.836791 kcal mol^{-1} in bulk

2.3.2. Propagation of EHMA

In the case of EHMA (analogous to MHMA) the *trans* monomer with a hydrogen-bond between the hydroxyl group and the carbonyl oxygen is the most stable conformer as expected and shown by Degirmenci *et al.* [28]. The structure of bulk EHMA has been analyzed by Antonucci *et al.* [35] who claim that EHMA forms a 6-membered ring structure via intramolecular H-bonding (Figure 2.6). Infra-red (IR) spectroscopy of EHMA shows that the carbonyl stretching peak occurred at a lower wavenumber (1712 cm^{-1}) than that of monomers which bear a carbonyl group, such as HEMA (1719 cm^{-1}). The lower wavenumber (longer bond) for EHMA is an indication that hydrogen-bonding is stronger overall. Harmonic frequencies computed for several hydrogen-bonding modes of EHMA were compared to experimental IR wavenumbers [35] (Figure 2.6). Computed harmonic frequencies were scaled by a factor of 0.9636 to account for the finite basis set employed, as well as the neglect of anharmonic effects and electron correlation [67]. In line with experimental findings, intermolecular hydrogen bonding clearly reduces the computed carbonyl wavenumber (1674 cm^{-1} and 1679 cm^{-1} in Figure 2.6 a and c, respectively) as compared to the computed wavenumber for free carbonyl (1694 cm^{-1}, for free carbonyl in EHMA-3, Figure 2.7). Calculations show that intermolecular hydrogen-bonding has a larger effect than intramolecular.

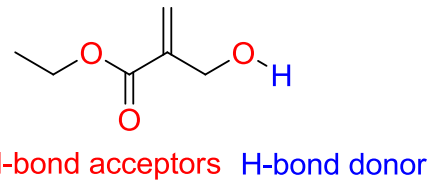

Figure 2.5. Hydrogen-bond donor and acceptor atoms in the EHMA monomer.

The attack of the *anti* radical (EHMA-R-2) to the *cis* monomer (EHMA-2) is most favored for syndiotactic addition, hence TS-EHMA-1 –with two intermolecular hydrogen-bonds (1.93 Å and 1.87 Å)– is more stable than the others. For the isotactic addition, attack of the *syn* radical (EHMA-R-2) to the *cis* monomer (EHMA-2) is preferred, hence, TS-EHMA-6 with two intermolecular hydrogen-bonds (2.01 Å and 2.04 Å) is the most favora-

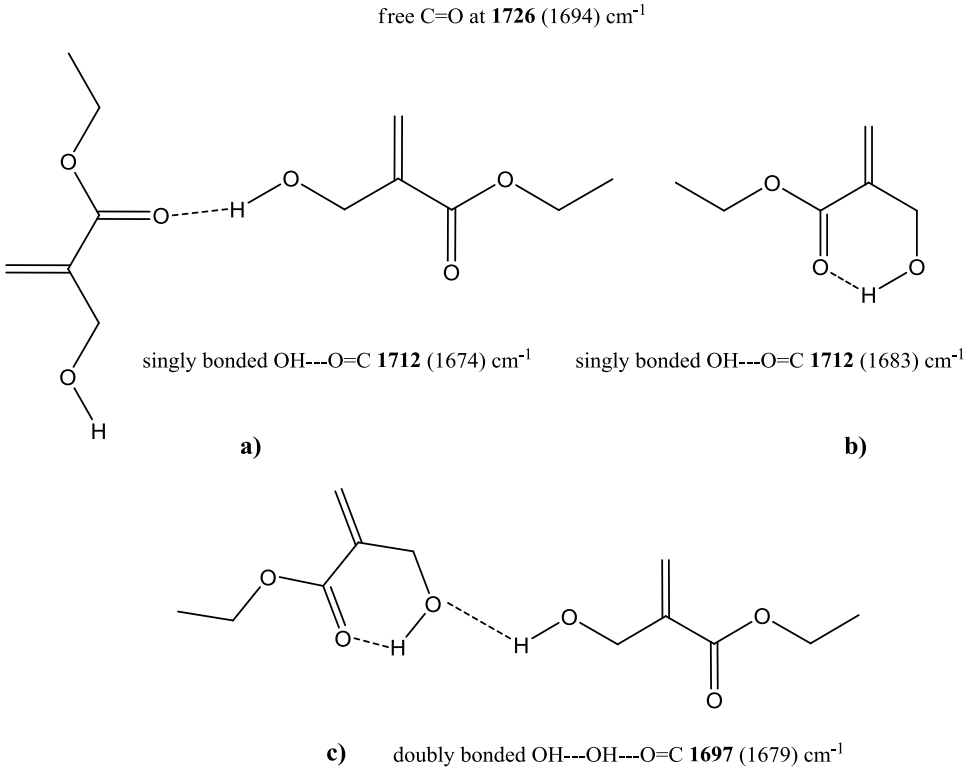

Figure 2.6. Hydrogen-bonding modes in the EHMA monomer monitored by Infra-Red (IR) Spectroscopy in bold [11]; computed harmonic frequencies (B3LYP/6-31+G(d)) are shown in parenthesis.

rable. Structures of all calculated transition states are shown in Figure 2.8.Here, the stability differences between transition states are more pronounced compared to those of EMA (Figure 2.4). The second energetically favored transition state after TS-EHMA-1 is TS-EHMA-2 which is also an intermolecular hydrogen-bonded transition state. Moreover, transition states with intramolecular hydrogen-bonds (TS-EHMA-3, TS-EHMA-5 and TS-EHMA-7) are less favored. Transition states with one intramolecular and one intermolecular hydrogen-bond (TS-EHMA-4 and TS-EHMA-8) are the least favorable; this could be due to the less stable s*yn* radical.

Monomers	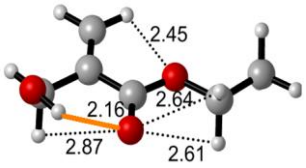	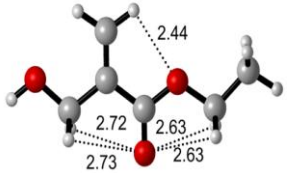	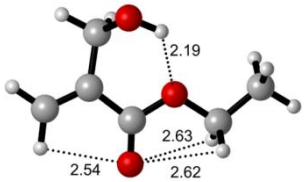	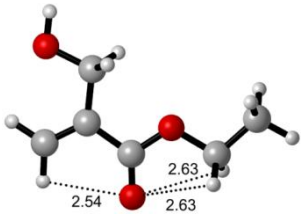
	EHMA-1	EHMA-2	EHMA-3	EHMA-4
	0.00 (0.00)*	0.70 (0.42)	1.73 (1.13)	1.70 (1.05)
Radicals	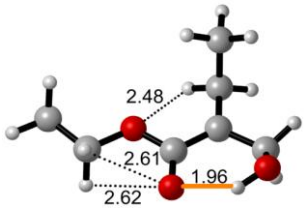	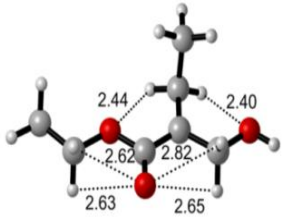	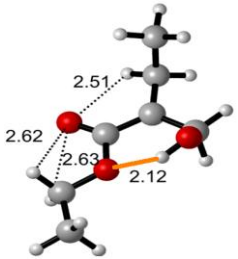	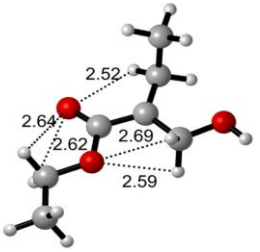
	EHMA-R-1	EHMA-R-2	EHMA-R-3	EHMA-R-4
	0.00 (0.00)**	1.27 (0.98)	1.33 (1.03)	1.64 (1.15)

Figure 2.7. Structures and relative Gibbs free energies of monomers and radicals of EHMA.

IEF-PCM (ε=7.80 for bulk EHMA) calculations in parenthesis. MPW1K/6-311+G(3df,2p)//B3LYP/6-31+G(d). Orange bonds show intramolecular H-bonds. * (HF+ZPG) = -460.207846 in gas, -460.214801 in bulk, ** (HF+ZPG) = -500.077895 kcal mol^{-1} in gas, -500.084861 kcal mol^{-1} in bulk.

Table 2.3. Gibbs free energies of activation (kcal mol^{-1}) for EHMA at 303K.[a,b]

					$\Delta G^{\ddagger}$	
	Tacticity	M	R	H-bonding	BMK[c]	MPW1K[d]
TS-EHMA-1	syn	*cis*	*anti*	MOH-RCO ROH-MCO	17.49 (17.16)	19.28 (18.93)
TS-EHMA-2	syn	*cis*	*syn*	MOH-RCO ROH-RCO	17.96 (18.17)	19.72 (19.92)
TS-EHMA-3	syn	*trans*	*anti*	MOH-MCO ROH-RCO	19.22 (19.51)	20.69 (20.98)
TS-EHMA-4	syn	*trans*	*syn*	MOH-MCO ROH-MEtO	21.02 (20.37)	22.23 (21.57)
Weighted average	syn				17.70 (17.37)	19.52 (19.17)
TS-EHMA-5	iso	*cis*	*anti*	MOH-MEtO ROH-RCO	21.09 (20.56)	22.35 (21.82)
TS-EHMA-6	iso	*cis*	*syn*	MOH-RCO ROH-MCO	18.25 (18.19)	20.32 (20.24)
TS-EHMA-7	iso	*trans*	*anti*	MOH-MCO ROH-RCO	21.50 (20.90)	21.90 (21.31)
TS-EHMA-8	iso	*trans*	*syn*	MOH-RCO ROH-REtO	21.04 (20.27)	22.58 (21.81)
Weighted average	iso				18.32 (18.33)	20.53 (20.56)
Weighted average	*Overall*				17.80 (17.50)	19.63 (19.32)

[a]BSSE corrections included. [b]IEF-PCM calculations (ε=7.80 for bulk EHMA) in parenthesis. [c]BMK/6-311+G(3df,2p)//B3LYP/6-31+G(d). [d]MPW1K/6-311+G(3df,2p)//B3LYP/6-31+G(d). M: monomer; R: radical; MOH: monomer hydroxyl; ROH: radical hydroxyl; MCO: monomer carbonyl; RCO: radical carbonyl; MEtO: monomer ethoxy; REtO: radical ethoxy.

Syndiotactic	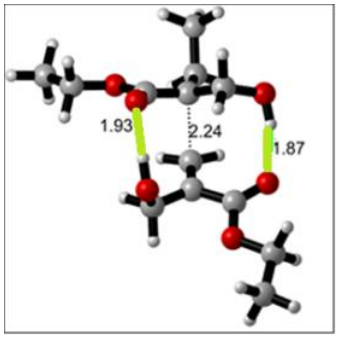	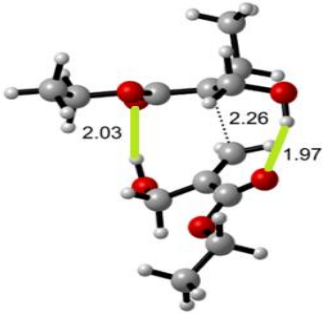	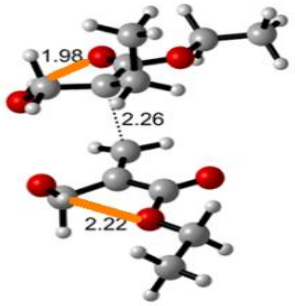	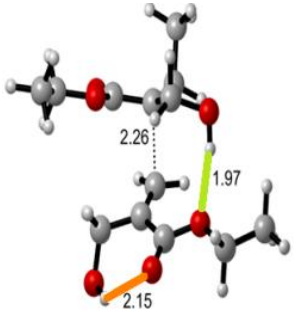
	TS-EHMA-1	TS-EHMA-2	TS-EHMA-3	TS-EHMA-4
	0.00 (0.00)*	0.44 (0.98)	1.41 (2.05)	2.95 (2.64)
Isotactic	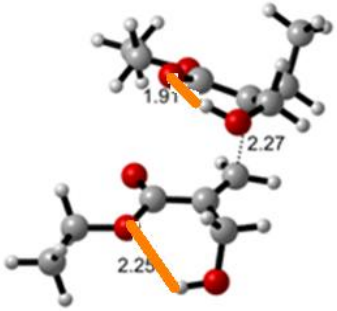	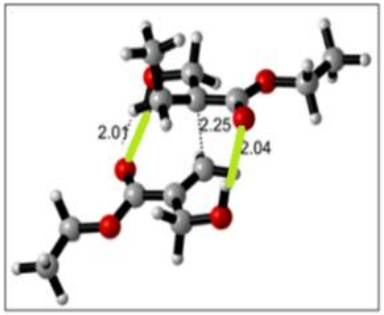	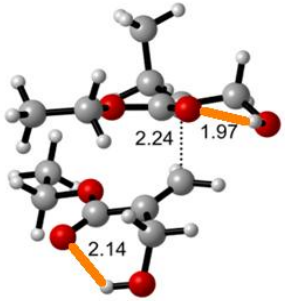	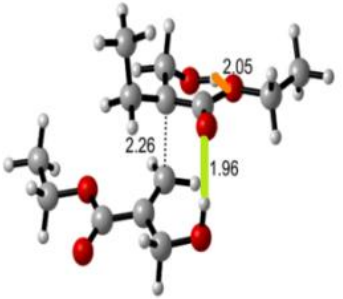
	TS-EHMA-5	TS-EHMA-6	TS-EHMA-7	TS-EHMA-8
	3.07 (2.89)	1.04 (1.31)	2.62 (2.38)	3.30 (2.88)

Figure 2.8. Structures and relative Gibbs free energies (BSSE corrections included) of the transition states of EHMA.

IEF-PCM (ε=7.80 for bulk EHMA) calculations in parenthesis. MPW1K/6-311+G(3df,2p)//B3LYP/6-31+G(d). Orange bonds show intramolecular H-bonds, green bonds show intermolecular H-bonds. *(HF+ZPG) = -960.255012 kcal mol^{-1} in gas, -960.266466 kcal mol^{-1} in bulk.

Beuermann *et al.* [25, 26] have explained the free radical polymerization behavior of hydroxypropyl methacrylate HPMA and have suggested that the hydrogen-bonds that are already present between the monomer between monomers and macromolecules during the polymerization. This statement supports our findings in a way that the transition states of EHMA with intermolecular hydrogen-bonds are more stable than those with intramolecular hydrogen-bonds.Degirmenci *et al.* [28] also studied the propagation behavior of EHMA in gas phase, taking into account intermolecular hydrogen-bonding possibilities between the monomer and radical; they have reported that transition states with intramolecular hydrogen-bonds (TS-EHMA-3, Figure 2.8) are energetically more favorable compared to intermolecular hydrogen-bonded transition states. However, they only considered the possible attacks of the most stable radical to the most stable monomer; herein all possible combinations are considered as shown in Figure 2.3. The current study shows that hydrogen-bonds between the monomer carbonyl and the radical hydroxyl significantly stabilizes the transition state and this conformation is only possible if the monomer is *cis* instead of the more stable conformation, *trans*. Overall the intermolecular hydrogen-bonded transition state (e.g.TS-EHMA-1, Figure 2.8) is found to be energetically more favorable than the intramolecular hydrogen-bonded transition states e.g. TS-EHMA-3. Additionally, Davis *et al.* [31] have claimed that the interactions between the monomer and propagating radical in the transition state may cause a tacticity preference in EHMA polymerization, in line with our results based on Gibbs free energy differences, which show that the free radical polymerization of EHMA is 85% syndiotatic.

2.3.3. Comparison of EMA and EHMA

Calculations in bulk (Table 2.4) show that k_p values for EHMA are higher than those for EMA, most probably due to the hydrogen-bonds that stabilize the transition structures of EHMA. Davis *et al*. claim that [31] that regardless of solvent effect, k_p of EHMA is more than 12-40 % higher than k_p of EMA. Thus considering the k_p of EMA as measured by Zammit *et al*. [33] in bulk together with the measurements of Davis *et al*. for EHMA, yields a $k_{p(EMA)}/k_{p(EHMA)}$ ratio of 0.35. Note that, Davis *et al*. expect k_p of EHMA in bulk to be higher than the one in ethanol, so the $k_{p(EMA)}/k_{p(EHMA)}$ ratio should actually be lower than 0.35; thus experimental trend has been reproduced qualitatively with calculations. In the

case of EHMA, due to the presence of intermolecular hydrogen-bonding, the propagating species are closer to each other and this facilitates the reaction.

Table 2.4. Weighted averages of Gibbs free energies of activation (kcal mol^{-1}) and propagation rate constants (L $mol^{-1}s^{-1}$) in bulk for EMA and EHMA within the IEF-PCM model.

		EMA	EHMA	$k_{p\ (EMA/EHMA)}$[e]
BMK[c]	$\Delta G^{\ddagger}$	21.17 (19.94)	17.80 (17.50)	0.004 (0.017)
	k_p	0.09 (0.66)	22.99 (37.76)	
MPW1K[d]	$\Delta G^{\ddagger}$	21.80 (20.52)	19.63 (19.32)	0.027 (0.135)
	k_p	0.03 (0.25)	1.10 (1.86)	

[a]BSSE corrections included. [b]IEF-PCM calculations (ε=3.00 for bulk EMA, ε=7.80 for bulk EHMA) in parenthesis. [c]BMK/6-311+G(3df,2p)//B3LYP/6-31+G(d). [d]MPW1K/6-311+G(3df,2p)//B3LYP/6-31+G(d). [e] The predicted experimental $k_{p(EMA)}/k_{p(EHMA)}$ ratio as explained in text is 0.35.

2.3.4. *EHMA polymerization in ethanol and toluene*

For EHMA, the intermolecular hydrogen-bonded transition state structure geometry, TS-EHMA-1 (syndiotactic) is the most stable one (Figure 2.8). This structure has been used to calculate the k_p values in toluene (ε=2.37) and ethanol (ε=24.85). The first two rows of Table 2.5 display the kinetic results with the continuum solvent model IEFPCM where the two solvents toluene and ethanol, have been considered implicitly. The ratio of k_p*'s* in toluene and ethanol ($k_{p\ (toluene)}/k_{p\ (ethanol)}$) qualitatively reflects the experimental ratio (first row of Table 2.6) but is slightly higher than expected. Due to ethanol's hydrogen bonding potential, an investigation of the role of explicit ethanol molecules in the polymerization of EHMA is therefore more than desirable. However, many hydrogen-bonding possibilities exist in the transition state; hydrogen-bond donor groups that are taken into account are the monomer and radical hydroxyl groups; hydrogen-bond acceptors are the monomer and radical carbonyl groups. TS-EHMA-1 was chosen for further explicit solvation by ethanol, since it represents the lowest energy transition structure.

Ethanol H-bonds with radical	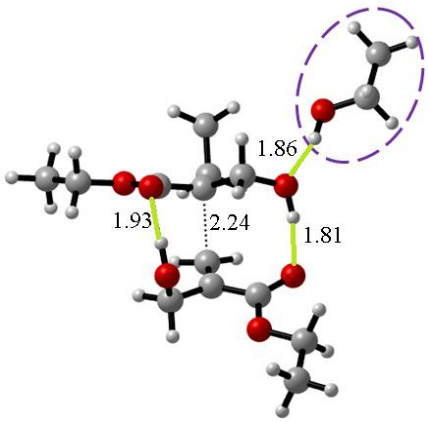	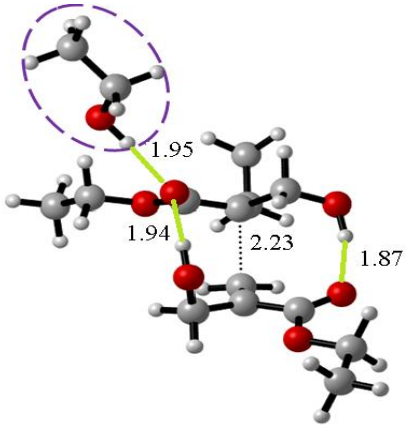
	TS-EHMA-1-r1	TS-EHMA-1-r2
	0.00 (0.00)*	1.39 (0.57)
Ethanol H-bonds with monomer	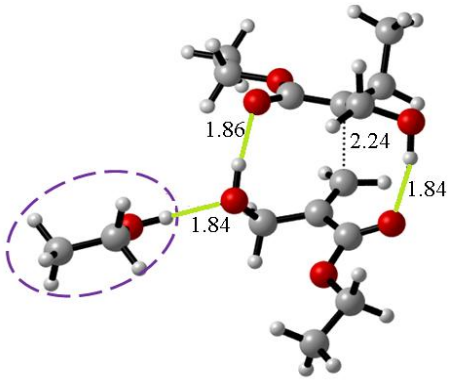	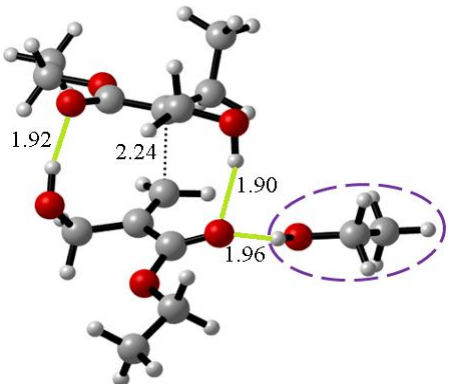
	TS-EHMA-1-m1	TS-EHMA-1-m2
	-0.08 (1.33)	1.81 (2.08)
Ethanol forms bridge between radical and monomer	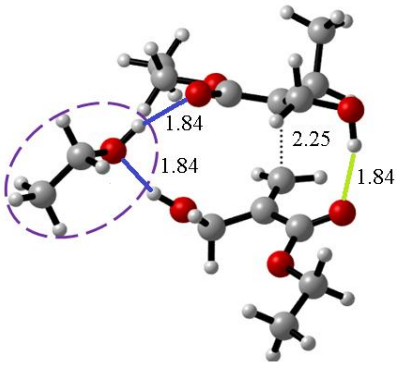	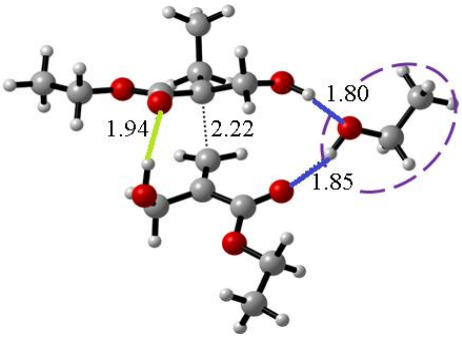
	TS-EHMA-1-b1	TS-EHMA-1-b2
	0.76 (2.47)	-1.82 (1.70)

Figure 2.9. Structures and relative Gibbs free energies (BSSE corrections included) of the transition state- solvent complexes of EHMA.

IEF-PCM (ε=24.85 for ethanol) calculations in parenthesis. MPW1K/6-311+G(3df,2p)// B3LYP/6-31+G(d). Green bonds: intermolecular H-bonding and ethanol H-bonds to monomer or radical, blue bonds show bridging H-bonds. * (HF+ZPG) = -114.245955 kcal mol^{-1} in gas, -115.260643 kcal mol^{-1} in implicit ethanol.

To be able to calculate k_p with explicit ethanol molecules, the optimum positions at which ethanol can hydrogen-bond to the monomer or/and the radical have been considered. As shown in Figure 2.5, there are three H-bond acceptor oxygen atoms and one H-bond donor hydrogen atom in the monomer and the radical. Ethanol is also both a hydrogen-bond acceptor and donor, therefore, all possibilities were considered. As seen in Figure 2.9, an ethanol bridging the radical and the monomer (TS-EHMA-1-b1 and TS-EHMA-1-b2) does not further stabilize these structures since the bridging ethanol ruptures intermolecular hydrogen bonds between the monomer and the radical, which seem to be preferred over hydrogen-bonds with ethanol. After optimizing the complexes, the supermolecule is further immersed in a continuum solvent environment; k_p is calculated to see the effect of both explicit and implicit solvent on the propagation rate constant (Table 2.5). Since the relative Gibbs free energy differences of the transition states are rather small, all combinations have been considered and the weighted average of Gibbs free energies of activation for all transition states with explicit ethanol molecules have been taken into account. The ratio of $k_{p(toluene)}/k_{p(ethanol)}$ with explicit/implicit ethanol and implicit toluene is tabulated in Table 2.6.

Experimentally one notices some decrease in k_p upon dilution with ethanol (Table 2.1). The more ethanol molecules are present in the reactive media, the larger the disruptive effect of ethanol in rupturing or weakening the intermolecular H-bonds between the monomer and the radical, which results in a slight decrease of the reaction rate. On the other hand, the opposite is observed with toluene as solvent; the propagation rate k_p increases with increasing amount of toluene. This is entirely consistent with the idea that toluene cannot interrupt favorable hydrogen-bonds between the monomer and the radical in the transition state, the propagating species are closer to each other when surrounded by hydrophobic toluene molecules and the rate increases. The slightly larger propagation rate for toluene is well described by the calculations (Table 2.6). On the quantitative level the

experimental ratio of 2.40 (Table 2.1) is even correctly reproduced if the ethanol solvent molecules are explicitly taken into consideration.

As already mentioned by Beuermann [68], Buback [69] and Radom [70] the effect of the solvent on the Arrhenius parameters- pre-exponential factor, *A* and activation energy, E_a -is of uttermost importance in order to rationalize the origins of the solvent effect. Table 2.7 displays the calculated (MPW1K/6-311+G(3df,2p)//B3LYP/6-31+G(d)) Arrhenius parameters of the free radical polymerization of EHMA in toluene and ethanol. The experimental Arrhenius parameters reported in Table 2.1 for EHMA in toluene (1:3) and ethanol (1:3) show that the 2.40 fold rate acceleration in toluene is partially due to the activation barrier (1.44 fold) but mainly due to the frequency factor (1.67 fold). The calculated Arrhenius parameters for ethanol and toluene show that the pre-exponential factor is mainly responsible for the rate acceleration in toluene (2.29 fold) as compared to the one in ethanol. In toluene, the EHMA monomers are stabilized by intramolecular H-bonding and tend to form 6-membered rings as displayed in Figure 2.6 or they can make H-bonds with each other. Toluene will not alter the arrangement of EHMA molecules whereas in ethanol these species will tend to make hydrogen bonds with the solvent and lose somewhat their compact ordered shapes: overall the reactants will be less ordered in ethanol.The transition structures in both media being more or less equally disordered the difference in entropy (disorder) between the transition structures and the reactants are expected to be smaller in ethanol. Thus the frequency factor which is measure of disorder between the transition structure and the reactants is expected to be higher in toluene. Our calculations attribute the 2.28 fold rate increase in toluene mainly to an increase in the frequency factor. This finding is slightly overestimated in the calculations as compared to experiment probably due to the small dimeric size of the model chosen as compared to the propagating long chain.

Table 2.5. Gibbs free energies of activation (kcal mol^{-1}) and propagation rate constants (L $mol^{-1}s^{-1}$) from explicit/implicit solvent calculations for EHMA in ethanol and toluene at 303K.[a]

	BMK[b]		MPW1K[c]	
	$\Delta G^{\ddagger}$	k_p	$\Delta G^{\ddagger}$	k_p
TS-EHMA-1 (implicit toluene)	16.58	175.23	18.22	11.54
TS-EHMA-1 (implicit ethanol)	17.31	51.65	19.08	2.76
TS-EHMA-1-r1	19.15 (16.42)	2.47 (229.62)	18.78 (18.25)	4.50 (10.97)
TS-EHMA-1-r2	19.21 (17.17)	2.23 (65.90)	18.93 (18.79)	3.51 (4.47)
TS-EHMA-1-m1	16.25 (18.07)	300.67 (14.70)	16.48 (19.85)	207.22 (0.76)
TS-EHMA-1-m2	16.98 (17.24)	90.13 (58.57)	17.80 (19.28)	22.97 (1.97)
TS-EHMA-1-b1	16.74 (17.59)	135.11 (32.78)	17.08 (19.67)	75.70 (1.03)
TS-EHMA-1-b2	17.87 (18.22)	20.58 (11.56)	18.31 (19.92)	9.94 (0.68)
Weighted average	16.57 (16.91)	176.96 (101.24)	16.83 (18.72)	115.49 (5.03)

[a]IEF-PCM calculations (ε=24.85 for ethanol) in parenthesis. [b]BMK/6-311+G(3df,2p)//B3LYP/6-31+G(d). [c]MPW1K/6-311+G(3df,2p)//B3LYP/6-31+G(d)

Table 2.6. Ratio $k_{p(toluene)/(ethanol)}$ of rate constants for EHMA in toluene and ethanol at 303K.

		BMK[a]	MPW1K[b]	Experimental[c]
$k_{p\ (toluene)}/k_{p\ (ethanol)}$	$Toluene_{imp}/Ethanol_{imp}$[d]	3.39	4.16	2.40
	$Toluene_{imp}/Ethanol_{exp-imp}$[e]	1.73	2.28	

[a]BMK/6-311+G(3df,2p)//B3LYP/6-31+G(d) [b]MPW1K/6-311+G(3df,2p)//B3LYP/6-31+G(d) [c]Rate constants are taken from reference 4 and 5 and reproduced in Table 1. [d]For $Toluene_{imp}/Ethanol_{imp}$: TS-EHMA-1 in continuum is considered for both toluene and ethanol (Table 5, first two rows). [e]$Toluene_{imp}/Ethanol_{exp-imp}$: TS-EHMA-1 in continuum is considered for toluene; for ethanol the weighted average of the explicit-implicit solvent model is considered (Table 5, last row, values in parenthesis).

Table 2.7. Kinetic parameters for EHMA in different media at 303 K.[a]

	E_a (kcal mol^{-1})	A (10^4 L $mol^{-1}s^{-1}$)	k_p (L $mol^{-1}s^{-1}$)
Toluene[b]	5.82	18.2	11.54
Ethanol[c]	5.78	7.42	5.03

[a] (MPW1K/6-311+G(3df,2p)//B3LYP/6-31+G(d)) [b]TS-EHMA-1, [c] weighted average values for the structures in Figure 5.

2.4. Conclusion

In this study, the free radical polymerization (FRP) behavior of EHMA in bulk, ethanol and toluene has been modeled and compared to the FRP of EMA in bulk. In agreement with experiment, the FRP of EHMA is found to be slightly accelerated in toluene as compared to ethanol. Ethanol can explicitly interact with the propagating EHMA monomers, destroying their regular 6-membered ring shape via hydrogen bonding.

The solvent ethanol destroys the order of the reactants, decreasing the entropy of activation as compared to the same reaction in toluene which is hydrophopic. These results explain the experimentally observed dilution effects with both solvents: dilution with ethanol decelerates the reaction –due to the disruptive effect of ethanol– whereas dilution with toluene accelerates the reaction because of the hydrophobic nature of the solvent. EMA, which is known to have a slightly smaller gel effect than MMA, is commercially used in bulk and its polymerization behavior has been compared to the one of EHMA. Calculations predict the qualitative rate accelerating behavior of EHMA as compared to the EMA and reproduce qualitatively the experimental trend justifying the usage of the dimeric models proposed in this study for further qualitative understanding of the relative free radical polymerization behavior of acrylate derivatives.

3. SEQUENCE DEPENDENCE OF DEAMIDATION OF ASPARAGINE RESIDUES

3.1. Introduction

Initially it was thought that only peptides and proteins to deamidate are the ones with Asn or Gln residues followed by glycine (Gly) residues [71]. After a while, it has been argued that other Asn or Gln containing peptides and proteins are also prone to deamidate. However, the rate of the reaction is higher if the residue next to the Asn or Gln is less bulky and/or it contains a hydroxyl group since the formation of succinimide derivative is easier [72].

Later, more studies have been carried out to understand the nature of the deamidation. The complete 648-pentapeptide set of all possible combinations of the sequences Gly-Xxx-Asn-Yyy-Gly and Gly-Xxx-Gln-Yyy-Gly, where Xxx and Yyy are any of the 20 naturally occurring amino acid residues were synthesized and deamidation rates were determined by Robinson. Deamidation rate was shown to be controlled primarily by the carboxyl side residue (Yyy) with smaller effects from the amino side residue (Xxx) [14].

In addition to experimental research carried out on the deamidation, there have been also several theoretical studies to understand the deamidation reaction better [73-77]. In these studies, alternative pathways for the formation of a succinimide ring have been studied by DFT [46]. One of the most cited pathways is the concerted backbone nitrogen attack to the carbonyl carbon and the formation the five-membered tetrahedral intermediate from which succinimide is formed, a two step pathway, asn→tet→suc (Figure 3.1).

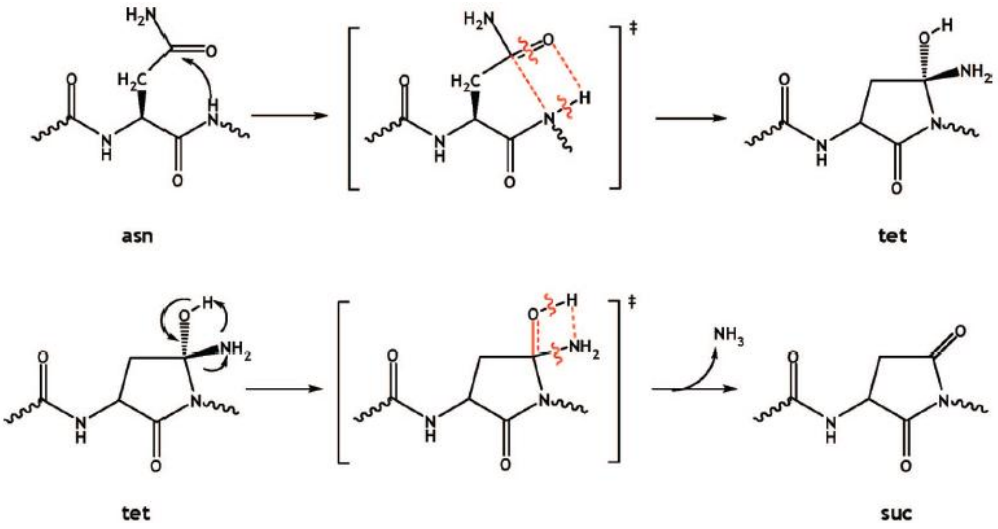

Figure 3.1. Formation of a succinimide ring via a tetrahedral intermediate [75].

An alternative pathway, a three step pathway, studied by Catak *et al*. is the tautomerization of the Asn side chain amide (Figure 3.2). In this pathway, it is suggested that firstly the amide on the side chain of the Asn residue tautomerizes and forms an amidic acid tautomer. Then this tautomer can form a five membered tetrahedral intermediate which subsequently results in the formation of succinimide ring via a three step pathway, asn→taut→tet→suc [73]. Nevertheless, the direct formation of the tetrahedral intermediate is found to be a competitive pathway since activation energies of the two reactions are close to each other.

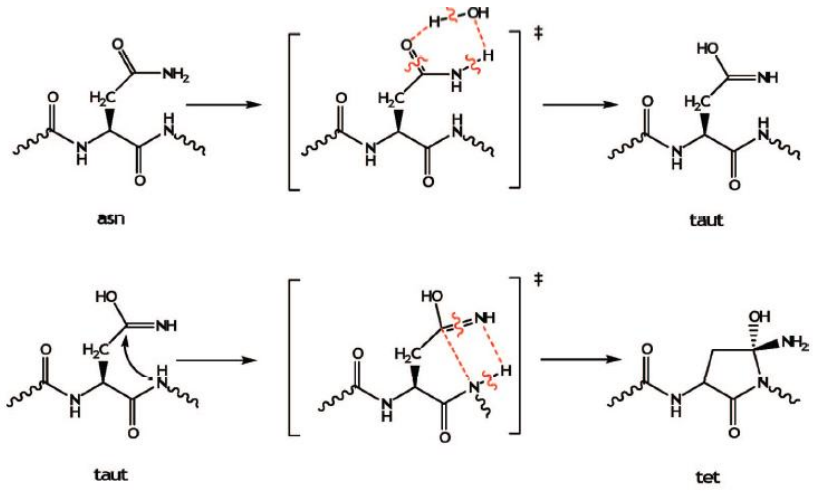

Figure 3.2. Three step pathway formation of succinimide ring formation via tautomerization route [75].

On the other hand, the direct formation of the succinimide intermediate, *asn* → *suc* pathway (Figure 3.3) is less likely to happen since the activation barrier for this reaction with B3LYp/6-31+G(d,f) is found to be quite high by Catak *et al*. [75].

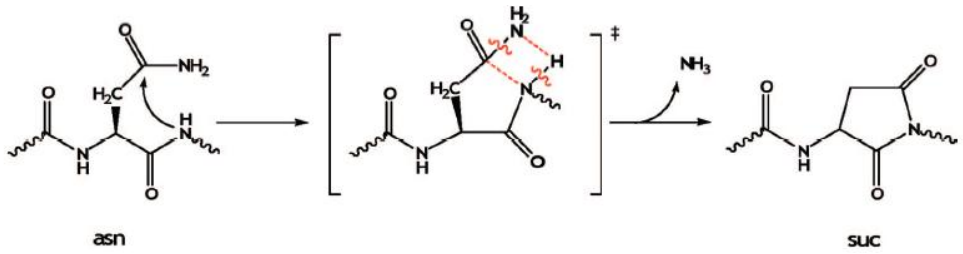

Figure 3.3. Direct formation of succinimide ring from Asn [75].

In this study, the experimental findings of Robinson *et al.* on the sequence dependence of the deamidation rates will be considered to understand the effect of sequence on deamidation rates [14]. The latter have determined the rates of 648 different pentapeptides with both Asn and Gln containing residues. However, here only Asn deamidation is considered since Gln deamidation is known to be much slower than Asn deamidation. In addition to that, it is known that residue on the amino terminus of the Asn (Xxx) does not affect the rate but the residue on the carboxyl terminus (Yyy) affects the rate. Therefore, to understand the effect of structure and sequence dependence of the rates, three different pentapeptides with different Yyy residues, Glycine (Gly), Methionine (Met) and Isolecuine (Ile) are taken as experimental reference peptides. It should be noted that only Yyy residues are different in the peptide models therefore the two ends of the pentapeptides are blocked by methyl groups (Figure 3.4) Although the tautomerization route is found to be the most possible pathway, here three possible pathways are studied with the peptide with Gly as n+1 residue: direct succinimide ring formation, tetrahedral formation mechanism and tautomerization mechanism.

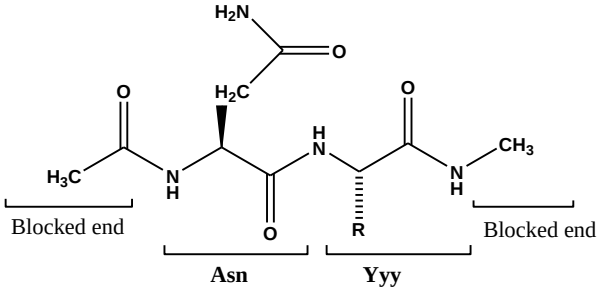

Figure 3.4. Model compound

Table 3.1. Deamidation half life and rate constants for the pentapeptides to be studied.

pH=7.4, 37°C	half life (days)	k (1/s)	$\Delta G^{\ddagger}$ (kcal/mol)
GlyGlyAsnGlyGly	1.03	7.79E-06	25.42
GlyGlyAsnMetGly	50.4	1.59E-07	27.81
GlyGlyAsnIleGly	287	2.80E-08	28.88

3.2. Computational Methodology

Full geometry optimizations were performed in gas-phase –without any constraints– using the density functional theory (DFT) [46] at the B3LYP/6-31+G** level [50, 78]. The use of this basis set and method in similar peptides systems is well established. Stationary points were characterized by a frequency analysis. Zero-point energy and thermal corrections were attained using the ideal gas approximation and standard procedures. Local minima and first-order saddle points were identified by the number of imaginary vibrational frequencies. The species reached by each transition structure were determined by intrinsic reaction coordinate (IRC) calculations [79]. Relative free energies of activation ($\Delta G^{\ddagger}$) are calculated as the difference of free energies between transition states and reactants (reactant-water complex where applicable) of each step. Energy values for gas-phase optimizations listed throughout the discussion include thermal free energy corrections at 310 K and 1 atm.

The self-consistent reaction field (SCRF) theory, utilizing the integral equation formalism-polarizable continuum (IEF-PCM) model [57-59] with UFF radii in water (ε = 78.0) at the B3LYP/6-31+G** level was used to account for the effect of a polar environment. Single point energies for solvent calculations include nonelectrostatic and thermal free energy corrections obtained from gas-phase optimizations.

All calculations were carried out using the Gaussian 09 program package [48] . All distances and free energies listed in the discussion are in angstroms (Å) and kcal/mol, respectively.

3.3 Results and Discussion

Primary sequence dependence of Asn deamidation is explored through the succinimide-mediated mechanism, which was modeled with different n+1 residues in order to see the differences in activation barriers. For this purpose, three end-blocked dipeptides, Asn-Yyy –where Yyy is Gly, Met and Ile– are used and modeled in light of the knowledge gained from previous computational studies on deamidation [14]. In the first part, three of the suggested pathways that leads to succinimide ring formation by Catak *et al*. [73, 75] have been studied for the end blocked dipeptide of Asn-Gly: *asn → suc; asn→tet→suc; asn→taut→tet→suc*. In the second part, the pathway with the lowest barrier is studied for the three end blocked peptides.

3.3.1. Deamidation of Asn-Gly sequence

The model compound shown in Figure 3.4 with Yyy residue being Gly is modeled, first the most stable conformer for the reactant is located (Figure 3.5). It is found that hydrogen bonds and also long range interactions stabilize the reactant. Note that the Gly residue and the blocked end nearby can freely rotate, however a seven membered ring via hydrogen bonding with the carbonyl oxygen of Asn residue forms instead.

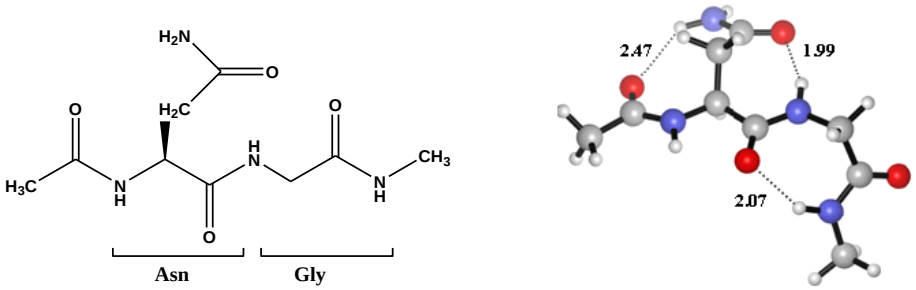

Figure 3.5. 2D and 3D structures of the Asn-Gly end blocked dipeptide, R-AG-1.

It has been shown by Konuklar *et al*.[76, 77] and Catak *et al*. [73-75] that it is necessary to study deamidation reaction with explicit water molecules. Thefore, all the mechanisms are studied here with explicit water molecules. Although it is desirable to add more explicit solvent water molecules since adding more explicit water has been shown to decrease the reaction activation barriers considerably, the qualitative picture does not change. The pathway that has the lower barrier-the rate determining step-does not depend on the number of explicit water molecules [75]. Therefore, only one explicit water molecule is added to the mechanism. It is also important to consider the synchronicity of the mechanism; concerted or stepwise. Catak *et al*. have studied both concerted and stepwise mechanisms for all three pathways. In this study, concerted and stepwise mechanisms are considered if at all possible.

In Figure 3.6, the geometries of reactant, transition state (TS) and products of direct succinimide ring formation pathway with explicit water are shown. The reactants and products are connected by IRC, the values in parentheses are calculated with the continuum solvent, IEFPCM with dielectric constant 78.5. Although this pathway, the formation of succinimide intermediate from asparagine residue is found to be a concerted step by Catak et al, we could not locate the concerted step. As seen from Figure 3.6, in the reactant R1-AG-suc the backbone amine proton of Gly deprotonates and this proton is transferred to the side chain amide nitrogen via a water molecule. Then, the succinimide ring is formed by cyclization via the attack of deprotonated nitrogen to the side chain carbonyl carbon atom.

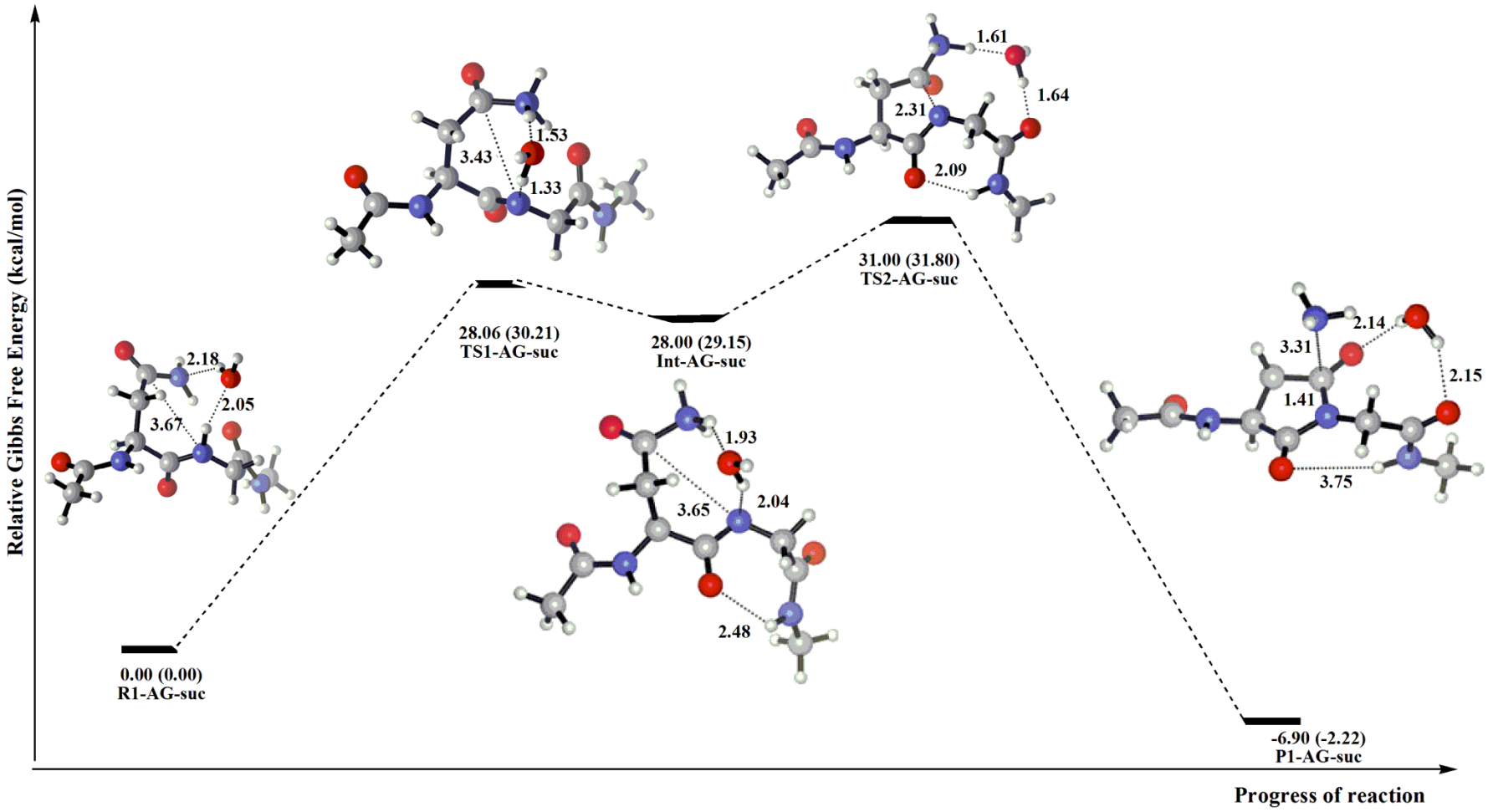

Figure 3.6. Potential energy graph for stepwise *asn* → *suc* route.

The second pathway studied is the tetrahedral intermediate formation via *asn→tet→suc* route (Figure 3.7). Here, the mechanism is found to be concerted, deprotonation of backbone amine group of Gly and the attack of the deprotonated nitrogen to the carbonyl carbon atom to form the tetrahedral intermediate occurs at the same time. However, it is seen that deprotonation occurs early in the reaction since in TS1-AG-tet, hydrogen transfer is seen to have already occurred to the side chain carbonyl oxygen atom.

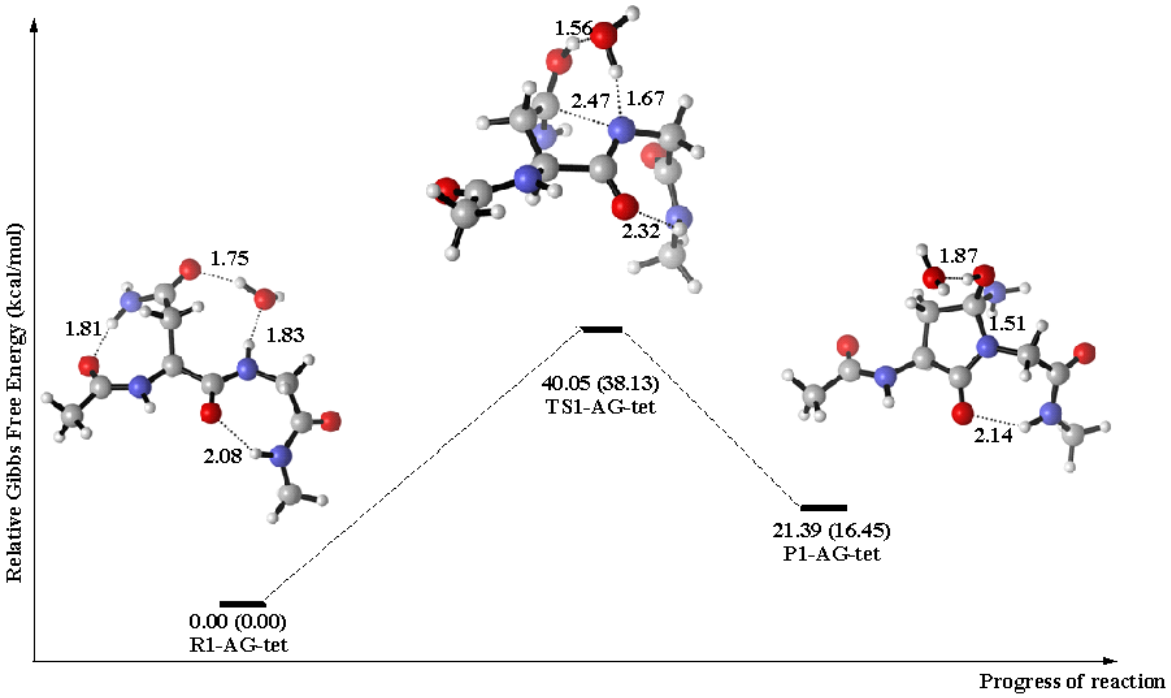

Figure 3.7. Potential energy graph for the concerted *asn→tet→suc* mechanism.

Finally, the tautomerization route, *asn→taut→tet→suc,* is studied (Figure 3.8-3.9). The first step tautomer formation is fast and concerted; the proton of the side chain amide is transferred to the carbonyl oxygen atom via water. After the formation of an amidic acid tautomer, a tetrahedral intermediate can be formed stepwise Here, we have located transition states for the stepwise mechanism as well. The deprotonation of Gly amino group via water and the transfer of the proton to double bonded side chain nitrogen occurs simultaneously. However, formation of the tetrahedral intermediate by the attack of the deprotonated nitrogen to the carbonyl carbon atom occurs after proton transfer.

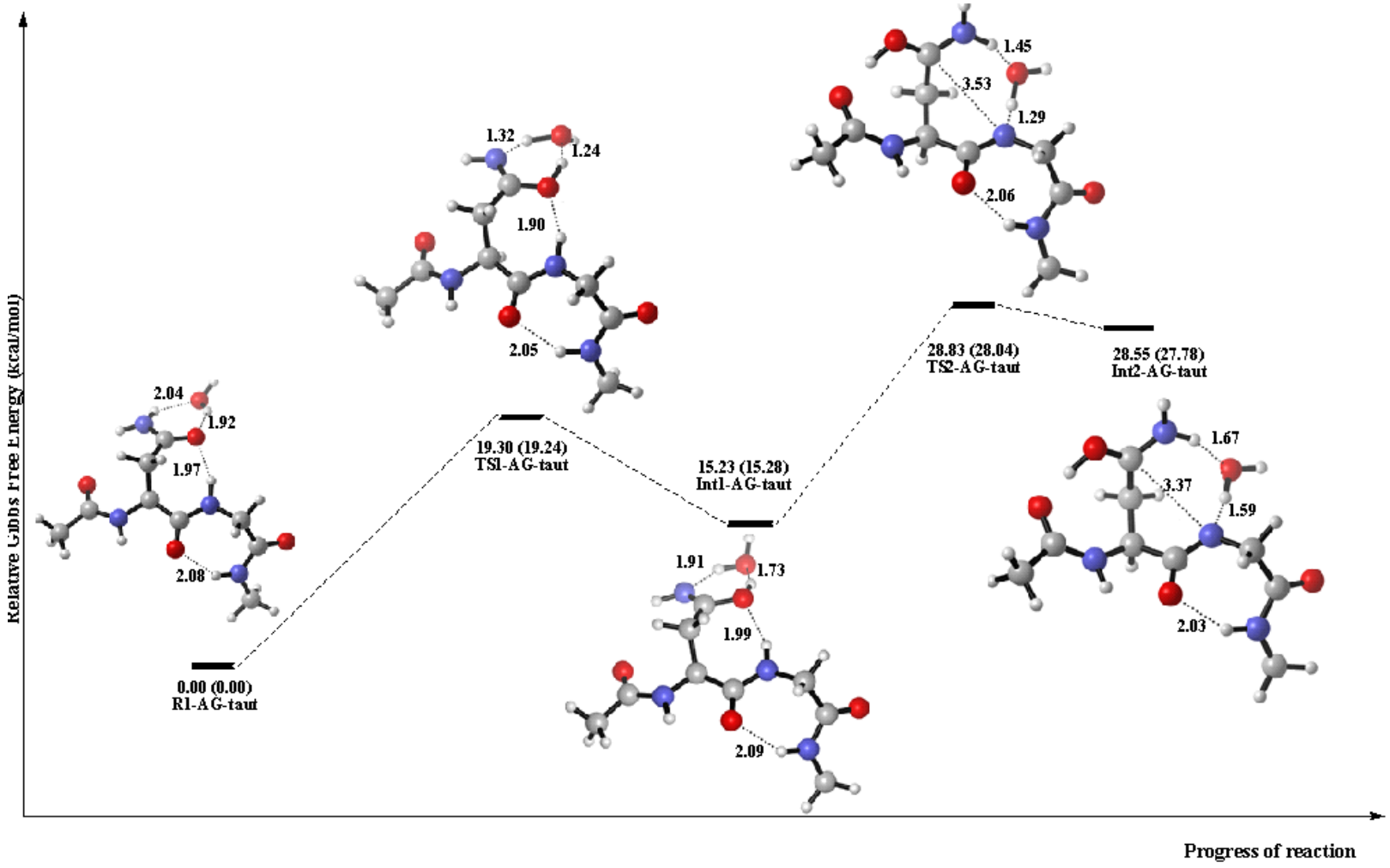

Figure 3.8. Potential energy graph of *asn→taut→tet→suc* route, proton transfer steps.

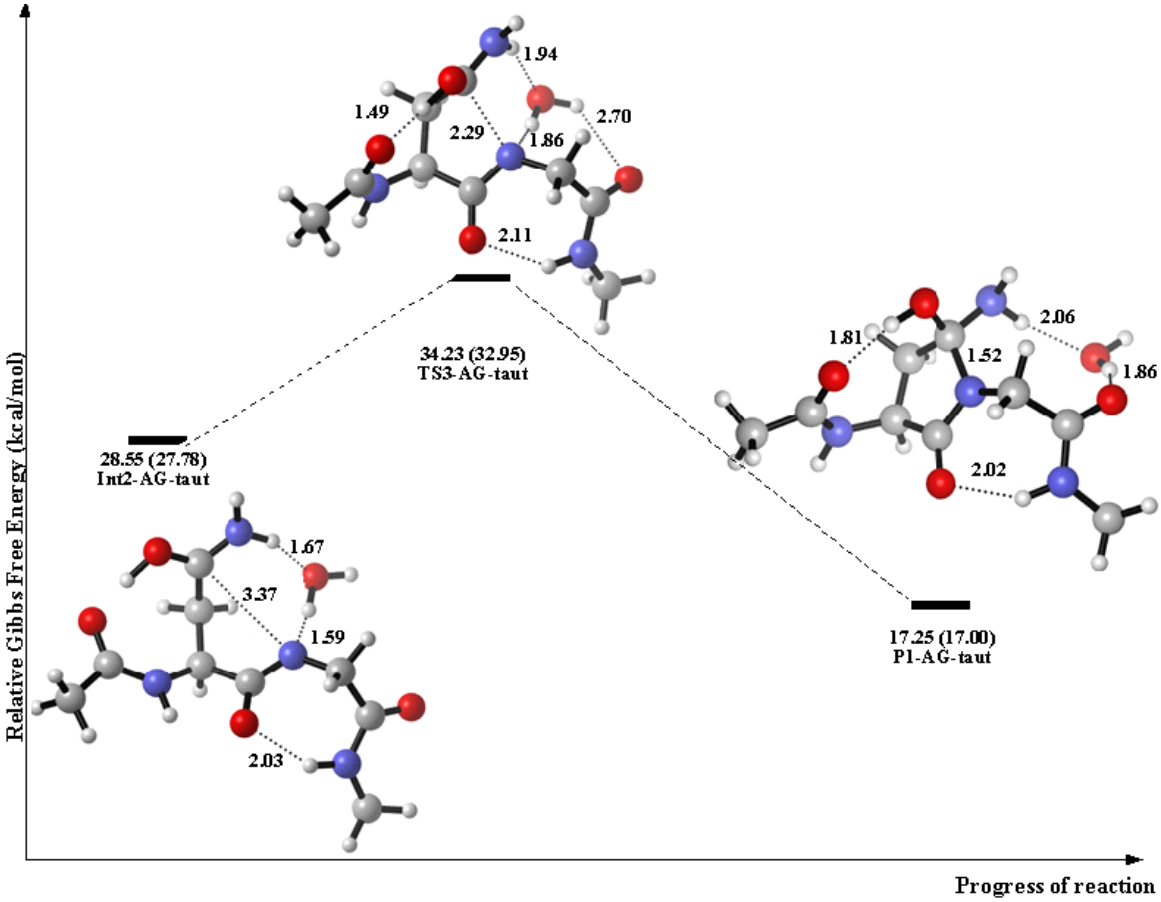

Figure 3.9. Potential energy graph of *asn→taut→tet→suc* route, cyclization step.

The structures and the barriers shown in Figure 3.6 – 3.9 are the IRC structures and barriers that connect the transition states to reactants and products may not realistic: the location of water molecules changes in all pathways. The most stable conformer of Asn-Gly dipeptide shown in Figure 3.4 and one water molecule are taken as reactants to calculate the barriers. In Table 3.2, the barriers of the cyclization step which is the attack of deprotonated nitrogen to the carbonyl carbon atom are shown since this step is known to be rate determining step. Note that here reactions are considered as bimolecular reactions.

It can be seen from Table 3.2 that tautomerization route is the most probable one since barrier is lower and then tetrahedral intermediate formation occurs. Direct succinimide formation has the highest barrier so it is the least plausible mechanism.

Table 3.2. Rate determining step barriers for three pathways

Pathway	$\Delta G^{\ddagger a}$
asn →suc	45.28 (46.03)
asn →tet→suc	40.88 (41.87)
asn→taut→tet→suc	35.70 (37.16)

[a] Energies are calculated with the B3LYP/6-31+G(d,f) methodology. The values in parentheses are for the continuum IEFPCM methodology with ε=78.5.

3.3.2. Comparison of deamidation rates of different sequenced peptides

The second part of the study is based on understanding the effect of the Yyy sequence on the deamidation rates (Figure 3.4). Here, direct succinimide ring formation will not be considered but tetrahedral ring formation with/without tautomerization will be taken into account. For deamidation to occur, atoms should be in certain geometry; dihedrals angles, angles and distances between atoms should be appropriate [76]. Therefore the differences between the barriers should be due to the stability of reactants and their structural differences due to the residues Yyy. As seen in Figure 3.10, there are reactive conformers of reactants which can be found along the potential energy graph by IRC and the most stable conformers of reactants correspond to the their actual geometry in the reaction media.

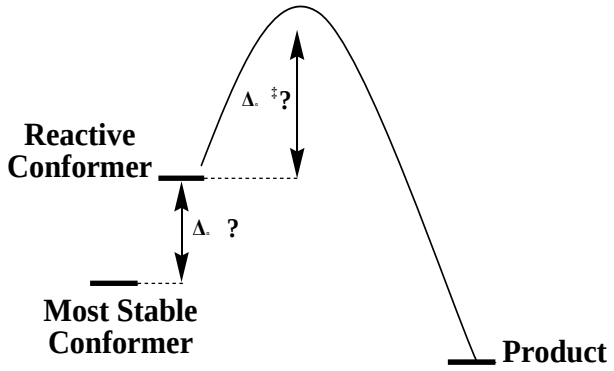

Figure 3.10. Potential energy surface for reactive and stable conformers.

The 2D structures for Asn-Gly, Asn-Met and Asn-Ile blocked ended dipeptides are shown in Figure 3.11. IRC calculations will be carried out to verify the nature of the reactants and products emerging from the transition states. Since it is evident that the last step of tautomerization route, cyclization step is the rate determining for *asn→tet→suc* mechanism, the transition state for this step (Figure 3.12) is modeled as well as the cyclization transition state (Figure 3.13) for the *asn→taut→tet→suc* pathway.

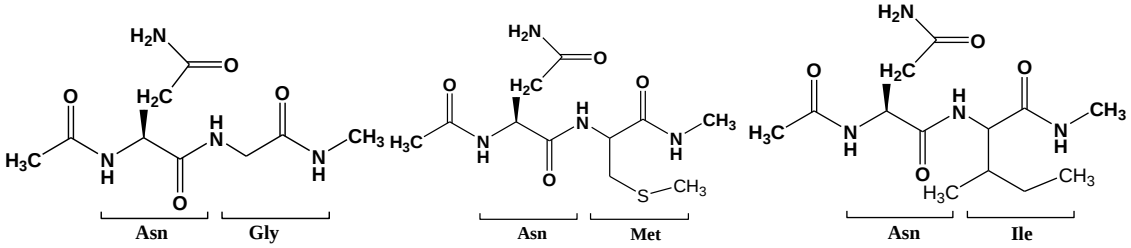

Figure 3.11. 2D structures of Asn-Gly, Asn-Met and Asn-Ile blocked dipeptides.

As can be seen from the structures of transition states for rate determining steps of tetrahedral intermediate pathway without tautomerization; *asn→tet→suc* pathway of Figures 3.12, the critical distances are a bit different from each other, (2.47 Å for TS1-AG-tet , 2.40 Å for TS1-AM-tet and 2.42 Å for TS1-AI-tet). However they are still close to each other and the stabilizing interactions are again similar. For tautomerization route, as can be seen from Figure 3.13, the geometries and critical distances (2.29 Å for TS3-AG-taut, 2.29 Å for TS3-AM-taut and 2.24 Å for TS3-AI-taut) are very close to each other. In all the transition states hydrogen bonds stabilize the structures.

However, it is evident from experimental data in Table 3.1 that primary sequence changes the rate of the deamidation. As explained in the first paragraph of this part, the difference between the deamidation rates of three dipeptides is expected to be due to the structure difference between most stable conformers of dipeptides. Therefore a conformer search is done to find the most stable forms of the reactants. In Figure 3.14 these structures are shown without explicit water molecules. Here, for consistency and comparability we think of the reaction as bimolecular so that different pathways can be compared easily. The activation Gibbs free energy which is shown as $\Delta G^{\ddagger}$ is actually the Gibbs free energy

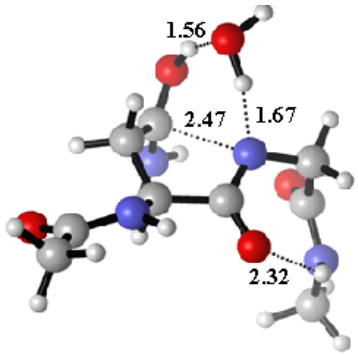

TS1-AG-tet

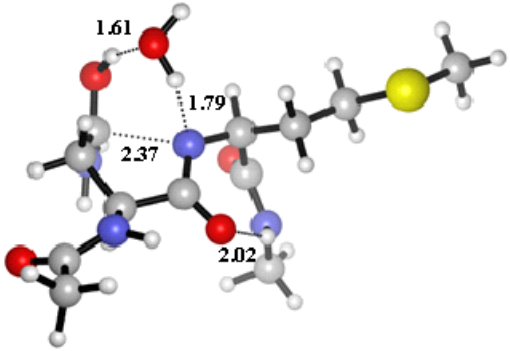

TS1-AM-tet

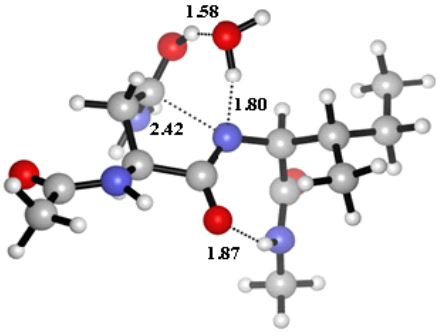

TS1-AI-tet

Figure 3.12. Cyclization Transition States for the dipeptides in the *asn→tet→suc* pathway.

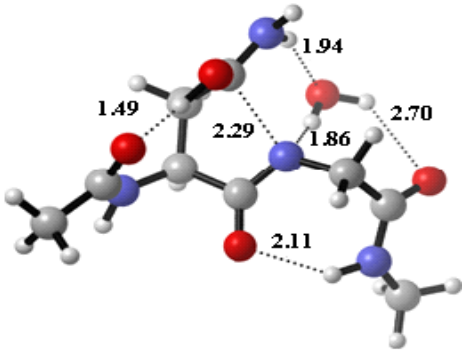

TS3-AG-taut

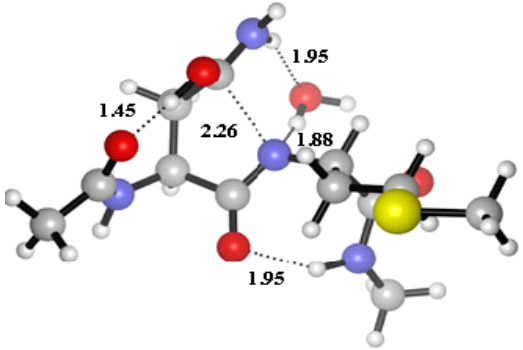

TS3-AM-taut

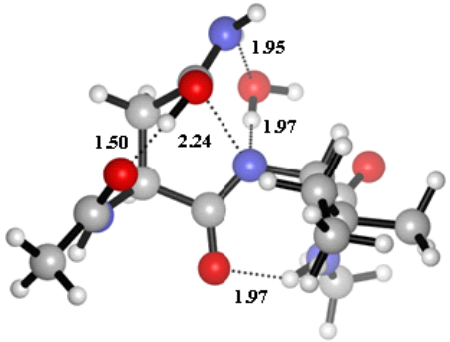

TS3-AI-taut

Figure 3.13. Cyclization Transition States for the dipeptides in the *asn→taut→tet→suc* pathway.

difference between reactive conformer and transition state. There is also the Gibbs free energy difference ΔG between the conformers of reactants; the sum of these two activation energies actually gives the barrier as shown in Figure 3.10.

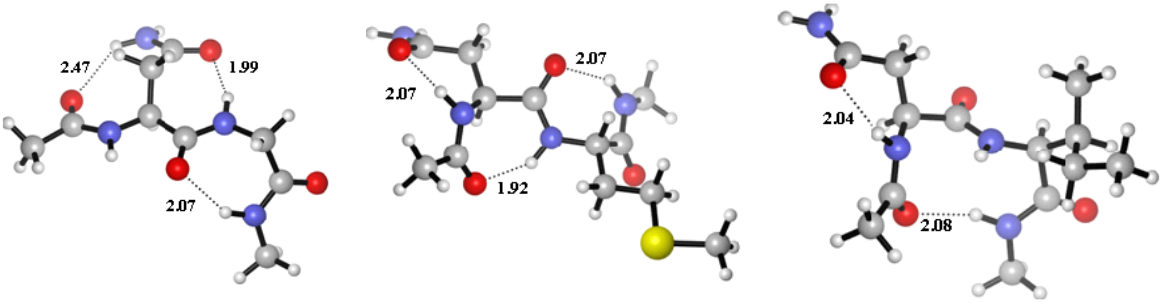

R-AG-1 R-AM-1 R-AI-1

Figure 3.14. Structures of the most stable reactants for three dipeptide models: Asn-Gly, Asn-Met and Asn-Ile.

Table 3.3. Energetics for different deamidation reactions

		Asn-Gly	Asn-Met	Asn-Ile
asn→tet→suc[a]	$\Delta G^{\ddagger}$	35.70 (37.16)	34.97 (39.06)	34.19 (31.30)
	ΔG	0.00 (0.00)	0.82 (-0.1)	4.06 (14.67)
	Total barrier	35.70 (37.16)	35.79 (38.95)	38.25 (44.08)
asn→taut→tet→suc[a]	$\Delta G^{\ddagger}$	40.88 (41.87)	38.41 (41.06)	42.83 (37.28)
	ΔG	0.00 (0.00)	0.82 (-0.1)	4.06 (14.67)
	Total barrier	40.88 (41.87)	39.23 (40.95)	46.89 (50.06)
experimental[b]	$\Delta G^{\ddagger}$	25.42	27.81	28.88

[a] B3LYP/6-31+G(d,f) is used, the values in parentheses are for IEFPCM calculations with ε=78.5. [b] Experimental values are taken from ref [14] and calculated with the transition state theory (TST).

It can be seen from Figure 3.14 that we could not find a more stable reactant for Asn-Gly dipeptide model, the most stable conformer, R-AG-1 and reactive conformer is found to be same. For Yyy = Met with a large R group ($-CH_2-CH_2-S-CH_3$) the most stable conformer is different from the reactive conformer. This difference is probably due to the

entropy increase, the most stable reactant for Asn-Met is more disordered. In the most stable conformer of Asn-Met reactant, the hydrogen bonds are actually between the backbone atoms and the large R group is far away from the backbone which decreases the steric hindrance. The same argument is true for Asn-Ile dipeptide model, here actually the difference between the most stable and reactive conformer is larger. This is expected since the R group (CH_3-CH_2-CH-CH_3) is bulkier. Due to this bulkiness the R group is away from the backbone to decrease the steric effects. From Table 3.3, it is seen that experimental trend is qualitatively reproduced, the tautomerization route gives lower barriers than the tetrahedral intermediate route without tautomerization. The calculated barriers and experimental barriers are quite different from each other, however it should be noted that only one explicit water molecule is used. Should two or more explicit water molecule are to be used, the barrier will become lower as seen in the example of Catak *et al*. [75].

3.4 Conclusion and Future Work

In this project, the effect of primary sequence on the deamidation rates of pentapeptides is modeled and rationalized by using Density Functional Theory. The deamidation rates determined determined by Robinson *et al*. show that only the residue next to the Asn, on the C-terminus side (n+1) affects the rate of deamidation. Therefore, blocked ended dipeptide models are used instead of pentapeptides. The mechanism of the deamidation is studied according to previously studied mechanisms [75, 76]. Three different pathways are studied for the Asn-Gly model, however the direct succinimide ring formation is found to be unlikely, therefore for other two peptides Asn-Met and Asn-Ile only two pathways are considered: *asn→tet→suc* and *asn→taut→tet→suc.*

Our results show that the pathway with the tautomerization of side chain is found to be more likely however the other mechanisms are also competitive. In addition to that the results are qualitatively in agreement with the experimental trend; the Asn-Gly dipeptide has lower barrier, then Asn-Met and then Asn-Ile. It is shown that the difference is not due to the structural difference between transition state structures of three dipeptide models but the difference between the reactive conformer and the most stable conformer is the cause of the deamidation rate difference. This difference between reactant conformers is more

likely to be because of steric effects due to the change of R group of residue next to the Asn.

For future work, the mechanisms will be modeled with two explicit water molecules and also the M06-2X functional having the ability to take into account dispersive effects will be used to calculate energies. Furthermore, a more systematic study for the conformer search will be done to confirm the nature of the most stable reactant conformers. In addition, the chain will be elongated; which means that instead of blocked dipeptide model, tripeptide or maybe tetrapeptide model will be used.

REFERENCES

1. Odian, G., *Principles of Polymerization*, Wiley Interscience, New York, 1991.

2. Satoh, K. and M. Kamigaito, "Stereospecific Living Radical Polymerization: Dual Control of Chain Length and Tacticity for Precision Polymer Synthesis", *Chem. Rev.*, Vol. 109, pp. 5120-5156, 2009.

3. De Sterck, B., R. Vaneerdeweg, F. Du Prez, M. Waroquier and V. Van Speybroeck, "Solvent Effects on Free Radical Polymerization Reactions: The Influence of Water on the Propagation Rate of Acrylamide and Methacrylamide", *Macromolecules*, Vol. 43, pp. 827-836, 2010.

4. Seymour, R. B., *Introduction to Polymer Chemistry*, McGraw-Hill Book Company, New York, 1971.

5. Matyjaszewski, K. and T. P. Davis, *Handbook of Polymer Chemistry*, Wiley-Interscience Publication, New York, 2002.

6. Beuermann, S., "Solvent Influence on Propagation Kinetics in Radical Polymerizations Studied by Pulsed Laser Initiated Polymerizations", *Macromol. Rapid Commun.*, Vol. 30, pp. 1066-1088, 2009.

7. Olaj, O. F., I. Bitai and F. Hinkelmann, "The Laser-Flash-Initiated Polymerization as a Tool of Evaluating (Individual) Kinetic Constants of Free-Radical Polymerization .2. The Direct Determination of the Rate-Constant of Chain Propagation", *Makromolekulare Chemie-Macromolecular Chemistry and Physics*, Vol. 188, pp. 1689-1702, 1987.

8. Olaj, O. F. and I. Schnollbitai, "Laser-Flash-Initiated Polymerization as a Tool for Evaluating (Individual) Kinetic Constants of Free-Radical Polymerization .5.

Complete Analysis by Means of a Single Experiment", *Eur. Polym. J.,* Vol. 25, pp. 635-641, 1989.

9. Capasso, S. and S. Salvadori, "Effect of the Three-Dimensional Structure on the Deamidation Reaction of Ribonuclease A", *J. Pept. Res.,* Vol. 54, pp. 377-382, 1999.

10. Chibnall, A. C. and R. G. Westall, "Determination of Glutamine in the Presence of Asparagine", *Biochemical Journal,* Vol. 26, pp. 122-132, 1932.

11. Damodarm, M., "The Isolation of Glutamine from an Enzymic Digest of Gliadin", *Biochemical Journal,* Vol. 26, pp. 235-247, 1932.

12. Damodarm, M., G. Jaaback and A. C. Chibnall, "The Isolation of Glutamine from an Enzymic Digest of Gliadin", *Biochemical Journal,* Vol. 26, pp. 1704-1713, 1932.

13. Solstad, T. and T. Flatmark, "Microheterogeneity of Recombinant Human Phenylalanine Hydroxylase as a Result of Nonenzymatic Deamidations of Labile Amide Containing Amino Acids - Effects on Catalytic and Stability Properties", *Eur. J. Biochem.,* Vol. 267, pp. 6302-6310, 2000.

14. Robinson, N. E. and A. B. Robinson, "Prediction of Primary Structure Deamidation Rates of Asparaginyl and Glutaminyl Peptides through Steric and Catalytic Effects", *J. Pept. Res.,* Vol. 63, pp. 437-448, 2004.

15. Robinson, N. E. and A. B. Robinson, "Amide Molecular Clocks in Drosophila Proteins: Potential Regulators of Aging and Other Processes", *Mech. Ageing Dev.,* Vol. 125, pp. 259-267, 2004.

16. Takemoto, L. and D. Boyle, "Specific Glutamine and Asparagine Residues of Gamma-S Crystallin Are Resistant to in Vivo Deamidation", *J. Biol. Chem.,* Vol. 275, pp. 26109-26112, 2000.
17. Watanabe, A., K. Takio and Y. Ihara, "Deamidation and Isoaspartate Formation in Smeared Tan in Paired Helical Filaments - Unusual Properties of the Microtubule-Binding Domain of Tau", *J. Biol. Chem.,* Vol. 274, pp. 7368-7378, 1999.

18. Robinson, N. E. and A. B. Robinson, "Prediction of Protein Deamidation Rates from Primary and Three-Dimensional Structure", *Proc. Natl. Acad. Sci. U. S. A.,* Vol. 98, pp. 4367-4372, 2001.

19. Robinson, N. E., Z. W. Robinson, B. R. Robinson, A. L. Robinson, J. A. Robinson, M. L. Robinson and A. B. Robinson, "Structure-Dependent Nonenzymatic Deamidation of Glutaminyl and Asparaginyl Pentapeptides", *J. Pept. Res.,* Vol. 63, pp. 426-436, 2004.

20. Anseth, K. S., S. M. Newman and C. N. Bowman, "Polymeric Dental Composites: Properties and Reaction Behavior of Multimethacrylate Dental Restorations", *Biopolymers Ii,* Vol. 122, pp. 177-217, 1995.

21. Decker, C., "Photoinitiated Crosslinking Polymerisation", *Prog. Polym. Sci.,* Vol. 21, pp. 593-650, 1996.

22. Kloosterboer, J. G., "Network Formation by Chain Crosslinking Photopolymerization and Its Applications in Electronics", *Adv. Polym. Sci.,* Vol. 84, pp. 1-61, 1988.

23. Avci, D. and S. H. Kusefoglu, "Functionalization and Cross-Linking Reactions of Ethyl-Alpha-Hydroxymethylacrylate", *J. Polym. Sci. Pol. Chem.,* Vol. 31, pp. 2941-2949, 1993.

24. Avci, D., S. H. Kusefoglu, R. D. Thompson and L. J. Mathias, "Ester Derivatives of Alpha-Hydroxymethylacrylates - Itaconate Isomers Giving High-Molecular-Weight Polymers", *J. Polym. Sci. Pol. Chem.,* Vol. 32, pp. 2937-2945, 1994.

25. Beuermann, S. and N. Garcia, "A Novel Approach to the Understanding of the Solvent Effects in Radical Polymerization Propagation Kinetics", *Macromolecules,* Vol. 37, pp. 3018-3025, 2004.

26. Beuermann, S. and D. Nelke, "The Influence of Hydrogen Bonding on the Propagation Rate Coefficient in Free-Radical Polymerizations of Hydroxypropyl Methacrylate", *Macromol. Chem. Phys.,* Vol. 204, pp. 460-470, 2003.

27. Degirmenci, I., D. Avci, V. Aviyente, K. Van Cauter, V. Van Speybroeck and M. Waroquier, "Density Functional Theory Study of Free-Radical Polymerization of Acrylates and Methacrylates: Structure-Reactivity Relationship", *Macromolecules,* Vol. 40, pp. 9590-9602, 2007.

28. Degirmenci, I., V. Aviyente, V. Van Speybroeck and M. Waroquier, "Dft Study on the Propagation Kinetics of Free-Radical Polymerization of Alpha-Substituted Acrylates", *Macromolecules*, Vol. 42, pp. 3033-3041, 2009.

29. Gunaydin, H., S. Salman, N. S. Tuzun, D. Avci and V. Aviyente, "Modeling the Free Radical Polymerization of Acrylates", *Int. J. Quantum Chem.,* Vol. 103, pp. 176-189, 2005.

30. Karahan, O., D. Avci and V. Aviyente, "Structure-Reactivity Relationships of Alkyl Alpha-Hydroxymethacrylate Derivatives", *J. Polym. Sci. Pol. Chem.,* Vol. 49, pp. 3058-3068, 2011.

31. Morrison, D. A. and T. P. Davis, "Studies on the Propagation Reaction in the Free Radical Polymerization of Ethyl Alpha-Hydroxymethacrylate", *Macromol. Chem. Phys.*, Vol. 201, pp. 2128-2137, 2000.

32. Ueda, M., T. Koyama, M. Mano and M. Yazawa, "Radical-Initiated Homopolymerization and Copolymerization of Ethyl Alpha-Hydroxymethylacrylate", *J. Polym. Sci. Pol. Chem.*, Vol. 27, pp. 751-762, 1989.

33. Zammit, M. D., M. L. Coote, T. P. Davis and G. D. Willett, "Effect of the Ester Side-Chain on the Propagation Kinetics of Alkyl Methacrylates - an Entropic or Enthalpic Effect?", *Macromolecules,* Vol. 31, pp. 955-963, 1998.

34. Smith, T. J., B. S. Shemper, J. S. Nobles, A. M. Casanova, C. Ott and L. J. Mathias, "Crosslinking Kinetics of Methyl and Ethyl (Alpha-Hydroxymethyl)Acrylates: Effect of Crosslinker Type and Functionality", *Polymer,* Vol. 44, pp. 6211-6216, 2003.

35. Antonucci, J. M., B. O. Fowler, M. D. Weir, D. Skrtic and J. W. Stansbury, "Effect of Ethyl-Alpha-Hydroxymethylacrylate on Selected Properties of Copolymers and Acp Resin Composites", *J. Mater. Sci.-Mater. Med.,* Vol. 19, pp. 3263-3271, 2008.

36. Cuervo-Rodriguez, R., V. Bordege, M. Sanchez-Chaves and M. Fernandez-Garcia, "Free-Radical Copolymerization of Ethyl Alpha-Hydroxymethylacrylate with Methyl Methacrylate by Reversible Addition-Fragmentation Chain Transfer", *J. Polym. Sci. Pol. Chem.*, Vol. 44, pp. 5618-5629, 2006.

37. Davis, T. P., M. D. Zammit, J. P. A. Heuts and K. Moody, "A Novel Route to the Preparation of Aldehyde End-Functionalised Oligomers Via Catalytic Chain Transfer Polymerisation", *Chem. Commun.,* Vol. pp. 2383-2384, 1998.

38. Blaker, J. W., "Concentric Bifocal Contact Lens with Two Distance Power Regions", US Patent 4752123, 1988.

39. Jansen, J., A. A. Dias, M. Dorschu and B. Coussens, "Fast Monomers: Factors Affecting the Inherent Reactivity of Acrylate Monomers in Photoinitiated Acrylate Polymerization", *Macromolecules*, Vol. 36, pp. 3861-3873, 2003.

40. Kilambi, H., J. W. Stansbury and C. N. Bowman, "Deconvoluting the Impact of Intermolecular and Intramolecular Interactions on the Polymerization Kinetics of Ultrarapid Mono(Meth)Acrylates", *Macromolecules*, Vol. 40, pp. 47-54, 2007.

41. Lee, T. Y., T. M. Roper, E. S. Jonsson, C. A. Guymon and C. E. Hoyle, "Influence of Hydrogen Bonding on Photopolymerization Rate of Hydroxyalkyl Acrylates", *Macromolecules*, Vol. 37, pp. 3659-3665, 2004.

42. Lemon, M. T., M. S. Jones and J. W. Stansbury, "Hydrogen Bonding Interactions in Methacrylate Monomers and Polymers", *J. Biomed. Mater. Res. Part A*, Vol. 83A, pp. 734-746, 2007.

43. Hirano, T., T. Kamikubo, Y. Fujioka and T. Sato, "Hydrogen-Bond-Assisted Syndiotactic-Specific Radical Polymerization of N-Isopropylacrylamide: The Solvent Effect on the Stereo Specificity", *Eur. Polym. J.*, Vol. 44, pp. 1053-1059, 2008.

44. Holmes, R. G., F. A. Rueggeberg, R. S. Callan, F. Caughman, D. C. N. Chan, D. H. Pashley and S. W. Looney, "Effect of Solvent Type and Content on Monomer Conversion of a Model Resin System as a Thin Film", *Dent. Mater.*, Vol. 23, pp. 1506-1512, 2007.

45. Valdebenito, A. and M. V. Encinas, "Effect of Solvent on the Free Radical Polymerization of N,N-Dimethylacrylamide", *Polym. Int.,* Vol. 59, pp. 1246-1251, 2010.

46. Parr, R. G. and W. Yang, *Density Functional Theory of Atoms and Molecules*, Oxford University Press, New York, 1989.

47. Gaussian 03, Revision D.01, Frisch, M. J., Gaussian, Inc., Wallingford CT, 2004.

48. Gaussian 09, Revision B.01, Frisch, M. J., Gaussian, Inc., Wallingford CT, 2009.

49. Becke, A. D., "Density-Functional Exchange-Energy Approximation with Correct Asymptotic-Behavior", *Phys. Rev. A,* Vol. 38, pp. 3098-3100, 1988.

50. Becke, A. D., "Density-Functional Thermochemistry .3. The Role of Exact Exchange", *J. Chem. Phys.,* Vol. 98, pp. 5648-5652, 1993.

51. Boese, A. D. and J. M. L. Martin, "Development of Density Functionals for Thermochemical Kinetics", *J. Chem. Phys.,* Vol. 121, pp. 3405-3416, 2004.

52. Lynch, B. J., P. L. Fast, M. Harris and D. G. Truhlar, "Adiabatic Connection for Kinetics", *J. Phys. Chem. A,* Vol. 104, pp. 4811-4815, 2000.

53. Laidler, K. J. and M. C. King, "The Development of Transition-State Theory", *J. Phys. Chem.,* Vol. 87, pp. 2657-2664, 1983.

54. Pechukas, P., "Transition-State Theory", *Annu. Rev. Phys. Chem.,* Vol. 32, pp. 159-177, 1981.

55. Truhlar, D. G., B. C. Garrett and S. J. Klippenstein, "Current Status of Transition-State Theory", *J. Phys. Chem.,* Vol. 100, pp. 12771-12800, 1996.

56. Truhlar, D. G., W. L. Hase and J. T. Hynes, "Current Status of Transition-State Theory", *J. Phys. Chem.,* Vol. 87, pp. 2664-2682, 1983.

57. Cances, E., B. Mennucci and J. Tomasi, "A New Integral Equation Formalism for the Polarizable Continuum Model: Theoretical Background and Applications to Isotropic and Anisotropic Dielectrics", *J. Chem. Phys.,* Vol. 107, pp. 3032-3041, 1997.

58. Mennucci, B. and J. Tomasi, "Continuum Solvation Models: A New Approach to the Problem of Solute's Charge Distribution and Cavity Boundaries", *J. Chem. Phys.,* Vol. 106, pp. 5151-5158, 1997.

59. Tomasi, J., B. Mennucci and E. Cances, "The Ief Version of the Pcm Solvation Method: An Overview of a New Method Addressed to Study Molecular Solutes at the Qm Ab Initio Level", *Theochem-J. Mol. Struct.,* Vol. 464, pp. 211-226, 1999.

60. Barone, V. and M. Cossi, "Quantum Calculation of Molecular Energies and Energy Gradients in Solution by a Conductor Solvent Model", *J. Phys. Chem. A,* Vol. 102, pp. 1995-2001, 1998.

61. Kelly, C. P., C. J. Cramer and D. G. Truhlar, "Adding Explicit Solvent Molecules to Continuum Solvent Calculations for the Calculation of Aqueous Acid Dissociation Constants", *J. Phys. Chem. A,* Vol. 110, pp. 2493-2499, 2006.

62. Pliego, J. R. and J. M. Riveros, "The Cluster-Continuum Model for the Calculation of the Solvation Free Energy of Ionic Species", *J. Phys. Chem. A,* Vol. 105, pp. 7241-7247, 2001.

63. Jansen, H. B. and P. Ros, "Non-Empirical Molecular Orbital Calculations on the Protonation of Carbon Monoxide", *Chem. Phys. Lett.,* Vol. 3, pp. 140-143, 1969.

64. Liptak, M. D., K. C. Gross, P. G. Seybold, S. Feldgus and G. C. Shields, "Absolute Pk(a) Determinations for Substituted Phenols", *J. Am. Chem. Soc.,* Vol. 124, pp. 6421-6427, 2002.

65. Van Speybroeck, V., D. Van Neck, M. Waroquier, S. Wauters, M. Saeys and G. B. Marin, "Ab Initio Study of Radical Addition Reactions: Addition of a Primary Ethylbenzene Radical to Ethene (I)", *J. Phys. Chem. A,* Vol. 104, pp. 10939-10950, 2000.

66. Isobe, Y., K. Yamada, T. Nakano and Y. Okamoto, "Stereospecific Free-Radical Polymerization of Methacrylates Using Fluoroalcohols as Solvents", *Macromolecules,* Vol. 32, pp. 5979-5981, 1999.

67. Merrick, J. P., D. Moran and L. Radom, "An Evaluation of Harmonic Vibrational Frequency Scale Factors", *J. Phys. Chem. A,* Vol. 111, pp. 11683-11700, 2007.

68. Beuermann, S., M. Buback, P. Hesse and I. Lacik, "Free-Radical Propagation Rate Coefficient of Nonionized Methacrylic Acid in Aqueous Solution from Low Monomer Concentrations to Bulk Polymerization", *Macromolecules,* Vol. 39, pp. 184-193, 2006.

69. Buback, M., "Propagation Kinetics in Radical Polymerization Studied Via Pulsed Laser Techniques", *Macromol. Symp.,* Vol. 275, pp. 90-101, 2008.

70. Heuts, J. P. A., R. G. Gilbert and L. Radom, "A Priori Prediction of Propagation Rate Coefficients in Free-Radical Polymerizations: Propagation of Ethylene", *Macromolecules,* Vol. 28, pp. 8771-8781, 1995.

71. Sun, A. W., K. U. Yuksel and R. W. Gracy, "Relationship between the Catalytic Center and the Primary Degradation Site of Triosephosphate Isomerase - Effects of Active-Site Modification and Deamidation", *Arch. Biochem. Biophys.,* Vol. 293, pp. 382-390, 1992.

72. Capasso, S., L. Mazzarella, F. Sica, A. Zagari and S. Salvadori, "Kinetics and Mechanism of Succinimide Ring Formation in the Deamidation Process of Asparagine Residues", *J. Chem. Soc.-Perkin Trans. 2*, Vol. pp. 679-682, 1993.

73. Catak, S., G. Monard, V. Aviyente and M. F. Ruiz-Lopez, "Reaction Mechanism of Deamidation of Asparaginyl Residues in Peptides: Effect of Solvent Molecules", *J. Phys. Chem. A*, Vol. 110, pp. 8354-8365, 2006.

74. Catak, S., G. Monard, V. Aviyente and M. F. Ruiz-Lopez, "Computational Study on Nonenzymatic Peptide Bond Cleavage at Asparagine and Aspartic Acid", *J. Phys. Chem. A*, Vol. 112, pp. 8752-8761, 2008.

75. Catak, S., G. Monard, V. Aviyente and M. F. Ruiz-Lopez, "Deamidation of Asparagine Residues: Direct Hydrolysis Versus Succinimide-Mediated Deamidation Mechanisms", *J. Phys. Chem. A*, Vol. 113, pp. 1111-1120, 2009.

76. Konuklar, F. A., V. Aviyente and M. F. R. Lopez, "Theoretical Study on the Alkaline and Neutral Hydrolysis of Succinimide Derivatives in Deamidation Reactions", *J. Phys. Chem. A*, Vol. 106, pp. 11205-11214, 2002.

77. Konuklar, F. A. S., V. Aviyente, T. Z. Sen and I. Bahar, "Modeling the Deamidation of Asparagine Residues Via Succinimide Intermediates", *J. Mol. Model.*, Vol. 7, pp. 147-160, 2001.

78. Madura, J. D. and W. L. Jorgensen, "Abinitio and Monte-Carlo Calculations for a Nucleophilic-Addition Reaction in the Gas-Phase and in Aqueous-Solution", *J. Am. Chem. Soc.*, Vol. 108, pp. 2517-2527, 1986.

79. Gonzalez, C. and H. B. Schlegel, "An Improved Algorithm for Reaction-Path Following", *J. Chem. Phys.*, Vol. 90, pp. 2154-2161, 1989.